

Genesis of natural hydraulic fractures as an indicator of basin inversion

Qingfeng Meng, John Hooker, and Joe Cartwright

Department of Earth Sciences, University of Oxford, South Parks Road, Oxford, OX1 3AN, UK

meng.qingfeng@hotmail.com

ABSTRACT

Satin spar (fibrous gypsum) veins, which occur in evaporite basins worldwide, provide significant insights into host rock deformation and fluid flow, although the genetic mechanism remains obscure. Satin spar veins in the red marls of the Triassic Mercia Mudstone of the Bristol Channel Basin were characterized in the context of regional and local setting. The vein network in the Keuper Marl (lower Mercia) exhibits a lack of systematic cross-cutting between three distinct vein sets. Two sets of veins are observed in the overlying Tea Green Marl, with one set clearly crossing the other. The gypsum veins commonly contain a blocky median zone of multiple thin bands of host-rock inclusions and alabastrine gypsum crystals, exhibiting crack-seal patterns. Fibrous zones on either side of the median zone consist of pure parallel-aligned gypsum fibres that are oblique to vein walls, indicating a hybrid shear-extensional mode of vein widening. Veins developed within reverse-reactivated faults contain fibre lineations in the median zones and also on vein surfaces, suggesting a minimum of two phases of fault slip. The veins are interpreted to have formed as a result of overpressure in the low-permeability mudstones by tectonic compression during basin inversion, giving rise to the median zone.

Growth of gypsum fibres commenced when the initial fractures were completely sealed. The timing of vein formation is suggested to be Miocene, based on cross-cutting relationships with folds formed during the latest phase of basin inversion. Because the fractures initiated in response to fluid overpressures, they provide a useful analog to subsurface hydraulic fracture systems in low-permeability rocks subjected to tectonic compression. The fibrous widening of the veins post-dates their initiation and led to continued propagation and increased connectivity.

Key words: hydraulic fracture; mudstone; crack-seal; antitaxial vein; basin inversion; overpressure

1. Introduction

Gypsum ($\text{CaSO}_4 \cdot 2\text{H}_2\text{O}$) occurs in nature in a variety of polycrystalline forms (Machel, 1985). Satin spar is a fibrous variety of needle-like gypsum crystals filling fractures (Gustavson et al., 1994). Satin spar veins, consisting of numerous parallel-aligned gypsum fibres, are commonly present in evaporite beds of sedimentary basins worldwide (Gustavson et al., 1994; Warren, 2006; Cobbold et al., 2013). The veins mainly appear in Triassic and Neogene strata, which are times of vast evaporite production under a warm and dry climate (Cobbold et al., 2013). The host rocks are mostly mudrocks and evaporites, or less commonly carbonates (Nichols, 2009; Cobbold et al., 2013). Recently, satin spar veins have been found on Mars, which indicates aqueous fluid activities in the hosts (Squyres et al., 2012; Arvidson et al., 2014; Nachon et al., 2014).

Satin spar veins have received considerable attention because their geometry and texture can provide information of the paleostress states, host rock deformations, and paleo-hydrological systems of their host rocks (Cosgrove, 1993; Passchier and Trouw, 1996; Bons, 2000; Bons et al., 2012; Cobbold et al., 2013; Moragas et al., 2013). The similarities of satin spar veins in many

evaporite basins indicate that they could share a common origin (Gustavson et al., 1994). Although it is generally acknowledged that the formation of fibrous veins is related to fracture mechanics (Bons et al., 2012), no consensus exists about their genesis. Gustavson et al. (1994) proposed that extension fractures could be created by subsidence over areas of halite dissolution, followed by precipitation of satin spar crystals in the fractures. Tabakh et al. (1998) argued that satin spar veins are initiated from overlying sediment unloading and exhumation, which not only favours the generation of sub-horizontal fractures, but also the dissolution of evaporites and subsequent remobilization. Considering the predominant low-permeability host rocks and sulphate-rich fluid movement, more researchers suggested that satin spar veins formed as natural hydraulic fractures that are cemented by gypsum from gypsum-saturated brines (Cosgrove, 2001; Philipp, 2008). The origin of overpressure is mainly attributed to tectonic compression by Cosgrove (2001), whereas Testa and Lugli (2000) and Philipp (2008) suggested that overpressure is more likely to result from anhydrite hydration and the associated solid-volumetric increase. However, Machel (1985) did not support the idea of anhydrite-gypsum transition in the host rocks as a prerequisite for the formation of satin spar veins. Instead, the author interpreted the veins to be tensile fractures either due to lateral tectonic compression, hydraulic overpressure, or a combination of the two factors. In a recent study, Rustichelli et al. (2016) subdivided satin spar veins into two types: (a) fault-related fractures in fault damage zones; and (b) bedding-parallel fractures formed by overpressure, which were later cemented by gypsum through diffusion.

This paper presents the field and petrographic study of the satin spar veins in the Triassic Mercia Mudstone of the Bristol Channel Basin that are exposed along the Somerset coast. A previous study of this area by Cosgrove (2001) suggested that the satin spar veins in the Mercia Mudstone

formed as natural hydraulic fractures during Cenozoic basin inversion. Fluid overpressure, which resulted from N-S tectonic compression, opened tensile fractures vertically against the minimum principal stress. Cosgrove interpreted that gypsum played a role only in the preservation of the veins, preventing their closure after overpressures ceased. Philipp (2008) supported the interpretation that the satin spar veins formed as hydraulic fractures, but attributed the overpressure to the hydration of anhydrite on the basis of the stratigraphic distribution of veins, ruptured nodules, and gypsum-lined faults. This paper presents additional observations to expand those provided in previous studies, particularly as regards the geometry and texture of the fibrous veins, which, we argue, imply a two-stage development. The aims of this paper are (1) to analyze the timing constraints of the satin spar veins in the marls; (2) to examine the mechanism of vein generation and its expression in vein microtextures; (3) to obtain a better understanding of the relationship between fault reactivation, fluid migration, pore pressure and the associated mineralization; and (4) to derive a general model for the formation of satin spar veins in low-permeability mudstones. The satin spar vein system in the Mercia Mudstone presented in this study constitutes an analogue to subsurface hydraulic fracture networks in mudstone.

2. Basinal context

The study area is located on the southern margin of the Bristol Channel Basin (BCB) (Fig. 1). The approximately E-W trending BCB extends from Wales to Somerset, 155 km E-W and 30 km N-S (Nemčok et al., 1995). The BCB was initiated in the early Permian to Triassic as an extensional basin developed around the south of England due to the breakup of the Pangaea (Kamerling, 1979; Van Hoorn, 1987; Brooks et al., 1988; Roberts, 1989; Coward, 1995). The BCB experienced extension and subsidence through the Triassic and Jurassic (Miliorizos and Ruffell, 1998), which led to the development of approximately E-W trending and southward-

dipping normal faults (Donato, 1988; Peacock and Sanderson, 1999). These basin-controlling normal faults were detached on a major Variscan thrust fault at depth that was reactivated and controlled the location and orientation of the normal faults (Donato, 1988; Peacock and Sanderson, 1991, 1994; Ruffell and Coward, 1992).

The main basin developed as a half graben bounded by the Bristol Channel Fault Zone (Kamerling, 1979; Brooks et al., 1988; Glen et al., 2005). During the Late Cretaceous to the Early Cenozoic, inversion occurred in the BCB as the result of N-S contraction caused by the Alpine orogeny (Van Hoorn, 1987; Peacock and Sanderson, 1992). The evidence for this phase of contraction comes from seismic profiles, field exposures of reverse-reactivated normal faults and strike-slip faults conjugate about a N-S orientation (Peacock and Sanderson, 1992, 1999). Most reverse-reactivated normal faults retain finite normal displacements; however, some faults changed into reverse faults (Peacock and Sanderson, 1992; Dart et al., 1995).

During the Permian and Triassic, the interplay of sea level change, extension-driven subsidence and climatic fluctuations significantly affected the sedimentation of the BCB (Ruffell and Shelton, 1999). Sediments deposited were typical of an arid environment including lacustrine red sedimentary rocks (Cosgrove, 2001), including conglomerate, sandstone, siltstone and mudstone (Whittaker and Green, 1983) (Fig. 2). During the Anisian, the Mercia Mudstone was deposited in subaqueous, hypersaline and evaporitic mudflats that replaced the southward retreating fluvial environment (Tucker, 1977; Dart et al., 1995). The Mercia Mudstone mainly consists of reddish-brown, less commonly green and grey, mudstones and marls with beds of halite in Somerset (Whittaker and Green, 1983; Howard et al., 2008). Subsequent transgression in the Late Triassic to Early Jurassic was accompanied by the deposition of grey to black marine mudstone of the

Lower Penarth Group and interbedded mudstones and thin limestones of the Blue Lias Group (Whittaker and Green, 1983; Howard et al., 2008).

3. Methods

Field observation along the cliffs was focused on vein shape, orientation, intersection, composition and texture. Vein orientation data were collected from nine randomly-selected sites using the 2D circular window method (one window per site), which could help comprise larger data sets and reduce sampling bias compared to linear scanline method (Mauldon et al., 2001). We gathered orientations of all veins within circular surfaces with a diameter of 1 m. Vein orientations were plotted by means of stereonet projection as great circles using Stereonet 9 software (Fig. 1A). Representative veins and their host rocks were sampled and cut into thin sections. Vein samples were deemed to be representative for petrographic analysis based on the fact that the veins exhibit a median suture of host rock inclusions with a finite width, and two outer zones of fibrous gypsum. The planes of thin sections are perpendicular to the plunge direction of fibres in veins, so that the true relative angle between fibres and vein walls could be observed. Microtextures of satin spar veins were characterized to provide clues for vein generation and cementation processes. Cross-cutting relationships between different sets of veins and between veins and other structures (faults, folds and sandstone dykes) were recorded to yield relative timing of the structures

4. Local setting

The study area is located in Warren Bay in the Watchet area, Somerset (Fig. 1). The coastal cliffs near Watchet mainly expose the Triassic strata of the Mercia Mudstone Group and the Lower Jurassic Blue Lias Formation (Figs 1, 2). The Mercia Mudstone is subdivided into the Keuper

Marl Formation and the Tea Green Marl Formation. The Keuper Marl is the oldest stratigraphic unit exposed, mainly consisting of red and brown featureless marls, occasionally green or grey siltstones, and few fossils. The Tea Green Marl Formation (TGM), also known as the Blue Anchor Formation, overlies the Keuper Marl and comprises laminated green-grey, red-brown dolomitic silty mudstone, and grey, black, green, and yellowish-grey dolostones.

Nodular gypsum is observed in multiple horizons in both the Keuper Marl and the TGM (Fig. 3A-B) where nodules are suggested to be generated as syndepositional evaporites in the capillary and upper phreatic zones beneath sabkha surface (Nichols, 2009). The depositional evaporites will experience a ‘gypsum-anhydrite-gypsum cycle’ (Murray, 1964), i.e. dehydrate to anhydrite when burial depth exceeds several hundred meters, and rehydrate to gypsum when it comes in contact with the low salinity, low-temperature pore waters on uplift to the telogenetic zone. Thus, diagenetically regenerated gypsum present as gypsum nodules and veins is regarded as secondary gypsum (Tucker, 2009).

Twelve sandstone dykes are observed in the Keuper Marl, mostly NNW-SSE striking with medium to high angle dips (37° - 84°) (Fig. 3) (Table 1). The sandstone dykes are composed of gypsum cemented, coarse sandstones that are compositionally identical to a sandstone body at the base of the Keuper Marl. Thus, the sandstone body is interpreted to have acted as the source of sand for the sandstone dykes. The dykes exhibit variable aperture ranging between 0.8-14.6 cm. The traces of the dykes are mostly curvy, which have been interpreted to be buckled hydraulic fractures formed during early burial and diagenesis (Cosgrove, 2001). A normal fault is observed to offset a sub-vertical sandstone dyke with a throw of 0.8m, whereas the correlative nodular horizons indicate a maximum fault throw of 2.1m (Fig. 3A). Some dykes contain dense gypsum veins, one of which includes a red host rock fragment trapped within the dyke (Fig. 3C-

D). This displacement difference suggests that the sandstone dyke was intruded later in the displacement history of the normal fault.

Numerous normal faults transect the outcrop of the Mercia Mudstone (Figs 1, 3A). These faults mostly strike E-W and NW-SE and dip at moderate to high angles (37° - 83°) (see supplementary material, Table S2). Three reverse faults cut the Mercia Mudstone in the study area with displacement ranging from 0.15 to 1.1m. Such faults are interpreted to be normal faults that were reactivated to accommodate the basin shortening (Kelly et al., 1999). The Blue Lias and the Mercia Mudstone outcrop in a horst that is bounded to the South by the E-W striking Helwell Bay Fault (Figs 1B, 4A). The horst is cut by the NW-SE striking Watchet Fault that transects the Mesozoic basin margin structures and possibly initiated as a Variscan structure (Holloway and Chadwick, 1986).

Buttress anticlines are observed in the hanging wall of reactivated normal faults (Fig. 4A) as the result of accommodation of basin shortening during Alpine compression and flexural flow with bed-parallel slip (Nemčok et al., 1995; Engelder and Peacock, 2001). The anticlines verge towards the horst and locally exhibit overturned forelimbs. The fold axes mainly strike NNW-SSE. Axial surfaces may dip as low as 20° . Intense buttressing occurs in the hangingwall of the Helwell Bay Fault to the east of the Watchet Fault, where complex parasitic anticlines and synclines develop around the crest. The folds are cut by numerous minor faults which are sub-parallel to the main faults. Detachment folds are observed in the Lower Lias strata of the horst, whose fold axes trend approximately E-W (Fig. 4B). The underlying evaporite beds of the TGM contain abundant nodular gypsum, and act as the décollement. The beds in the folds dip gently north, which increases sharply to be sub-vertical to the south.

5. Vein pattern

The red marls of the Keuper Marl expose dense networks of satin spar veins (Fig. 5A-D). The veins exhibit three preferred orientations, including the NW-SE striking and north dipping veins (K-1), E-W striking and south dipping veins (K-2), and sub-horizontal veins (K-3) (Figs 1, 5C). The veins of set K-1, dipping northward at 60°, are parallel to the E-W striking, basin-bounding normal faults along the southern margin of the basin. Those veins have been interpreted to be fault-controlled tectonic fractures (Cosgrove, 2001). The veins of set K-2 are parallel to the Helwell Bay Fault and many other normal faults exposed in the Warren Bay area. The sub-horizontal veins of set K-3 are sub-parallel to bedding planes.

Different veins in the Keuper Marl range from millimeters to tens of meters in length, and millimeters to 17 cm in aperture. The veins occur either as isolated individuals or as groups of closely-spaced veins with frequent intersections with adjacent inclined veins (Figs 5B, 5D). Small veins commonly exhibit tapering tips that pinch out in the marls, or curve towards neighboring veins. Sub-horizontal veins frequently occur as sets of en echelon veins (Fig. 6). The tips of neighboring veins commonly curve towards the neighboring vein and coalesce with them, hence trapping host rock fragments between vein tips. Similar features have also been observed by Virgo et al. (2014). Some sub-horizontal veins contain multiple parallel host-rock fragments, which are oblique to vein walls (Fig. 6D-H). Such veins are interpreted to result from coalescence of en echelon veins during lateral propagation.

The gypsum veins in the TGM exhibit distinctly different patterns from those in the Keuper Marl (Fig. 5E-F). The veins are more consistently oriented as two main sets, comprising an E-W striking, sub-vertical set (T-1) and a bedding-parallel set (T-2). Veins of set T-1 are pinkish-red

and quite evenly spaced (Fig. 5E). They commonly transect more than a single bed, with a height ranging from millimeters to approximately 2 m. Some of the pink veins exhibit sigmoidal shapes in the flat-lying beds of dolomites (Fig. 5F). The axial surfaces of those folds are approximately E-W striking. The curved veins are intact without signs of modifications. Veins of set T-2 are mainly concentrated in dark marls. These veins are white and bedding-parallel. White satin spar veins are also observed in the folds (Fig. 4A). The veins are predominately wavy. They may also exhibit a general sub-horizontal orientation and cross-cut multiple folded layers. This geometry indicates that the white veins postdate the folding of the host strata.

6. Texture and composition

The satin spar veins are mainly filled with fibrous gypsum crystals that are oblique to vein walls (Fig. 7A), indicating a shear component. The crystals are parallel-aligned and needle-like. Single fibres commonly exhibit an optical continuity, and remain constant in width (Fig. 7C-D). Fibrous gypsum crystals commonly exhibit high aspect ratios (up to 120). However, the values of aspect ratios vary in different veins, which is reflected in vein texture. Veins comprising crystals with aspect ratios <10 often exhibit an elongate-fibrous texture (Bons et al., 2012). Growth competition between crystals frequently occurs, with some crystals that overgrow others.

Most gypsum veins, especially the sub-horizontal veins, exhibit a thin band of median zone enclosed by upper and lower gypsum fibres (Fig. 7B-F). The median zone is not strictly located within the central part of the gypsum veins, and can be closer to either the upper or the lower vein walls (Fig. 7B, 7E). The median zone is mainly composed of host-rock inclusions. Locally, the median zone often contains large lenticular host-rock fragments with the long axes aligned sub-parallel to vein walls. Thin sections of satin spar veins reveal that the median zones have a

222 finite width. The median zone in single vein consists of multiple bands of wall-parallel host rock
223 inclusions and alabastrine gypsum, exhibiting an overall blocky texture (Fig. 7C-E). The gypsum
224 crystals are irregularly shaped and interlocked with neighbours. In veins with median zones,
225 fibres on the same side of the median zone share similar geometries and sizes, but exhibit
226 differences from those on the different side. Interestingly, fibres on one side commonly exhibit
227 smoother crystal boundaries than those on the other side. Overgrowth geometries frequently
228 occurs between crystals on the less-fibrous side.

229 Some satin spar veins do not contain median zones, and are fully filled with gypsum fibres that
230 continue from one wall to the other. Elongate-fibrous gypsum veins rarely have median zones.
231 Those veins are mainly composed of elongate-blocky crystals with long axes sub-orthogonal to
232 vein walls.

233 **7. Vein branching**

234 The satin spar veins commonly split into two or three branches during widening (Fig. 8). The
235 sum of aperture of the branches is similar to the original vein. One of the branches is often
236 parallel to the parent vein, and the other branch deviates from the original direction. The median
237 zone is only retained in one branch, and is not affected by vein branching and the change in vein
238 aperture. Interestingly, the bifurcations are not located in the median zone: they are in either the
239 upper or the lower fibrous zones in the veins (Fig. 8A-D). The apparent angles between the
240 branches and the parent veins varies from several degrees to almost ninety degrees.

8. Cross-cutting relationships

8.1. Differently Oriented Veins

Intersection of differently oriented gypsum veins is commonly observed in the red marls of the Keuper Marl, but no systematic cross-cutting of one set by another occurs. Although the intersecting veins are commonly seen as 'x' shaped geometries on cliff faces, they do not cross-cut one another (Fig. 9A-C). A representative scenario that can be misinterpreted as vein cross-cutting is shown in Fig. 9A. Coalescence occurs between sets K-1 and K-3. Vein *a* and *c* form an intact vein that exhibit smooth transitions at the nodes where vein-dip changes, so do vein *b* and *d*. Hence, vein *a* and *b* are unlikely to have formed as a single vein that was later modified. This interpretation is evident from the consistently oriented fibres in the veins, which are interpreted to have filled the horizontal and steep segments synchronously.

Fig. 9B shows intersections of three curved veins. Coalescence occurs between vein *a* and *b*, and also vein *a* and *c*. Vein *b* propagated towards the plane of vein *a*, which is indicated by the tapering tip to the left in the figure. Vein *c* is strongly curved, and it coalesces with vein *a* for 2 cm where the vein exhibits the maximum curvature. The coalescence of those veins results in a complex vein network.

Sub-horizontal veins, including branches, do not cross-cut steeply dipping veins (Fig. 9C). The tapering tips of sub-horizontal veins either coalesce with the steep veins or curve to follow their planes. Some steep veins are observed to occur as steps that link two adjacent horizontal veins (Fig. 9D). All veins share the same fibre orientations.

Some inclined veins are rooted in sub-horizontal veins, with the maximum aperture located in the bifurcation (Fig. 9E). The aperture of the inclined veins gradually decreases towards the host rock. The tips of such veins either pinch out or coalesce with adjacent sub-horizontal veins.

Thus, coalescence commonly occurs between differently oriented gypsum veins instead of cross-cutting where they intersect, which is especially common between veins of sets K-1 and K-3. In the Tea Green Marl, the red veins of set T-1 are clearly cross-cut by the bedding-parallel white veins of set T-2 with little offset (Fig. 5E).

8.2. Timing of Veins vs. Faults

The informal term ‘fault vein’ is used here to refer to veins that develop in a fault-parallel geometry within the fault zones of normal and reverse faults. Fault veins are observed to cross-cut sub-horizontal gypsum veins in two reactivated reverse faults, including the Helwell Bay Fault. The stratigraphy can be correlated from the hangingwalls to the footwalls of the two faults using the groups of nodular gypsum horizons and this correlation allows the recognition of offsets by faults of laterally extensive gypsum veins that share the same aperture, color and internal texture. Fig. 10A shows two closely spaced, horizontal veins offset by the paler fault vein with a fault throw of 92 cm. Fault veins are also observed to cross-cut veins in the host rock flanking the Helwell Bay Fault (Fig. 11A). The offset of the sub-horizontal white vein in the hangingwall and the footwall suggests a reverse motion with a throw of 12 cm. The needle-like fibres as mineral lineation are interpreted to mark the direction of dip slip.

In the majority of example faults, horizontal veins in the host rock are not cross-cut by faults, and instead the gypsum veins are seen to curve to follow the attitude of the fault planes (Fig.

11D). It is interpreted that such veins progressively propagated towards the faults from the adjacent areas and subsequently exploited the walls of fault veins as weak planes.

8.3. Timing of Veins vs. Folds

The gypsum veins in the intensively folded layers of the Blue Anchor Formation are commonly wavy, but their general orientations are sub-horizontal or slightly inclined. The veins frequently cut across the inclined beds regardless of the position and curvature of the folded layers (Figs 4A, 9H). Some veins have both sub-horizontal segments that cross-cut inclined beds, and also inclined segments that deviate from the horizontal direction to follow the bedding, often developing a wavy geometry. These wavy veins are observed to occur within beds of dark grey marls that are often tightly folded. Importantly, the fibre direction in these veins is consistently sub-vertical. If the wavy veins were folded with their host strata, we should instead observe a systematic rotation of the fibre directions across the folded layers. Hence, it can be concluded that vein formation postdated folding.

8.4. Timing of Veins vs. Sandstone Dykes

The sandstone dykes are considered as early-formed hydraulic fractures, based on their folded geometry. This timing is interpreted to result from post-intrusion compaction of the host mudstones (Cosgrove, 2001). The source sands must have been uncemented at the time of intrusion (Cartwright, 2010), and therefore, fluidized during early burial at a time when fluid overpressure was achieved, and when the differential stress was less than four times of the tensile strength of the marls (Cosgrove, 2001).

Additional evidence for the early timing of sandstone dykes is found from a normal fault that is observed to cross-cut a sub-vertical dyke (Fig. 3A). The intrusion of the dyke is interpreted to have occurred during the active period of the normal fault because the normal displacement of the dyke is less than that of the nodular gypsum horizons that occur at the same location.

The sub-horizontal gypsum veins are invariably seen to cross-cut the sandstone dykes (Fig. 3). Some gypsum veins curve to follow the dyke walls instead of cross-cutting them when they encounter the sub-vertical dykes (Fig. 3C-D). Hence, the sandstone dykes are interpreted to predate the gypsum veins.

9. Fault veins

All exposed faults of the Mercia Mudstone are cemented by gypsum (Figs 10-13) (Table S2). The E-W striking faults commonly expose slabs of white fault veins dipping north. The vein width varies from less than one centimetre to 16.8 cm. The median zones of the fault veins contain a large amount of host-rock inclusions and impure gypsum masses (Fig. 12A-B). Similarly to the satin spar veins in the rock matrix, the fault veins also contain two outer fibrous parts that are rather pure in composition (Fig. 12B-C).

Most faults exposed in the region are in net extension, whereas some faults show kinematic evidence for reverse reactivation (also see Glen et al., 2005). Fig. 10 shows a fault (F5) with a reverse displacement, and contains a 6 cm thick fault vein that exhibit a fibrous texture, and cross-cuts the horizontal gypsum veins in the bulk rock as a rare example of true cross-cutting. Importantly, lineations are observed on vein surfaces (Fig. 10B, 10D), which exhibit a sub-parallel direction to the fault plane. Those lineations are also parallel to striations on the surfaces of fault wall rocks (Fig. 10B-C). It is interpreted that the lineations are parallel to the sense of

slip. Depressions that are filled with centimetre-scale host rock fragments are observed on fault vein surfaces (Fig. 10D). Those rock fragments lie ahead of numerous fibres that exhibit a greater relief than the fragments, resulting in point asperities on vein surfaces. The fibre fronts also commonly exhibit irregular traces and varied surface reliefs, which are possible slickenside steps or the result of weathering.

Fig. 13 shows another reverse fault (F9) that contains a 4 cm thick gypsum fault vein. The fault vein consists of lineations in the median zone that lie parallel to the fault plane, and two outer fibrous parts. These fibres are sigmoidal-shaped, with the plunge gradually increasing to sub-normal towards vein walls (Fig. 13B). Lineations are observed on vein surfaces (Fig. 13C), which resemble those in the fault shown in Fig. 10D. The lineation front exhibits a crescent-shaped trace, which has a greater relief than the vein surface ahead and is interpreted as a slickenside step. Hence, the reverse slip of this fault is interpreted to be parallel to lineations on fault vein surfaces.

The gypsum cements developed in the fault zone of the Helwell Bay Fault appear as straight lineations lying within fault planes (Fig. 11). Those lineations are needle-like and coarser than those in the satin spar veins in the host rock (Fig. 11B). The fault vein offsets sub-horizontal veins in the marls (Fig. 11A), leaving fibre-parallel slickenlines on the sections of transected veins in the marls (Fig. 11C). Hence, the lineations in the fault vein are interpreted to form during the slip of the fault, which postdate the development of satin spar veins in the marls. Due to the severe weathering of the fault vein and the marls, it is difficult to obtain additional information of the sense of fault slip during the formation of the fibre lineations. However, according to the reverse displacement of the horizontal satin spar vein, it is interpreted that the lineations are associated with a reverse dip-slip of the Helwell Bay Fault. Such lineations in the

fault veins have formed either by means of syn-kinematic recrystallization or dissolution/precipitation (de Meer and Spiers, 1995, 1997; Fossen, 2010) that reshaped the gypsum crystals on vein surfaces in the direction of fault slip.

Based on the observations above, fault veins are interpreted to record at least two increments of displacement for faults in the study area (Fig. 14). During the first reverse reactivation of faults due to tectonic compression, lineations were produced on fault planes and aligned parallel to the fault slip direction. Such lineations are especially rich in the jogs that resulted from the asperities of fault planes. Those straight lineations serve as the median zone for the final fault veins. Then gypsum fibres start to grow towards vein walls during inactive periods of the faults. Finally, another phase of fault reverse reactivation commenced, with fibre lineations generated on vein surfaces that recorded the fault slip.

10. Discussion

10.1. Vein initiation by hydraulic fracturing

Satin spar veins in mudrocks have been suggested to form as hydraulic fractures (Shearman et al., 1972; Cosgrove, 1995, 2001) for the following reasons: (1) the formation of open-mode fractures relies on the fluid pressure to assist in pushing apart the wall rocks against the total rock pressure (Mandl, 2005); and (2) a vein fill of calcium sulphate requires the precipitation of gypsum from sulphate-rich fluids. The N-S tectonic compression during basin inversion, which is evident from fault reactivation and associated tight folding in the Watchet area (Figs 4, 11, 13), could have significantly contributed to the buildup of overpressure (c.f. Cosgrove, 2001). Due to the extremely low bulk permeability of the marls (Seedhouse and Racey, 1997), a pervasive increase of pore pressure Δp could occur because fluid cannot expel fast enough (Luo et al.,

2007; Couzens-Schultz and Azbel, 2014). The rise of pore pressure Δp reduces the effective stress to the point where tensile failure occurs resulting in hydraulic fractures (Mandl, 2005).

The initiation of vein opening by hydraulic fracturing is supported by observations of the textures of the satin spar veins. The gypsum veins in the study area exhibit typical characteristics of antitaxial veins (c.f. Durney and Ramsay, 1973; Cox, 1987). Median zones in such veins mark the initial site of fracturing and provide important information about how vein opened (Durney and Ramsay, 1973; Oliver and Bons, 2001; Bons and Montenari, 2005). Blocky textures of median zones were suggested to result from growth competition between crystals, which is likely to occur in open spaces (Fisher and Brantley, 1992; Bons, 2001), such as fluid-filled voids or fracture channels. It may be that gypsum precipitated into newly opened fractures because a concomitant drop in fluid pressure occurred that resulted in supersaturation. Or it may be that fracture opening produced a pore space large enough for already-supersaturated fluid to nucleate gypsum crystals. In either case, gypsum precipitation into hydraulic fractures partially or fully closed the fractures to fluid flow (Oliver and Bons, 2001). Therefore, the fracturing did not result in a general decrease in fluid pressure. Consequently, the fractures anneal, fluid pressure could then undergo a renewed increase (Oliver and Bons, 2001). Crack-seal texture indicates that the fractures were then reactivated and reopened as weak planes upon sufficient overpressure build-up. Pressure build-up could be the result of cyclic inversion stresses, erosional unloading during exhumation (c.f. Ingram et al. 2004), a high hydraulic head gradient at shallow depths, and/or a reduction of permeability in the mudrocks. In this way, the fluctuation in fluid pressure could result in repeated cracking in single veins (Barker, 2013).

Cracking preferentially occurs at vein-wall interfaces due to the low cohesion (Gale and Holder, 2010), which is accompanied with the introduction of one or two host rock inclusion bands.

Hence, the crack-seal mechanism (Ramsay, 1980; Cox and Etheridge, 1983; van der Pluijm, 1984; Laubach et al., 2004) is favoured in this study to explain the formation process of the median zone. Syntectonic strata buckling (Machel, 1985; Teixell et al., 2000) and sediment unloading (Mohamed El Tabakh and Warren, 1998; Teixell et al., 2000) could also contribute to the generation of sub-horizontal hydraulic fractures, where they exploit bedding planes and fissures as weak planes (Shearman et al., 1972). Another factor to be considered is that the veins formed within the gypsum stability field (see below) and therefore close to a free boundary, i.e. the surface. Overpressure could then be expected to form horizontal fractures, particularly if the near-surface stresses were horizontally compressive (e.g. Sheorey, 1994). The lack of median zones in some branches of satin spar vein suggests that vein branching occurred during incremental fibre growth and postdates the primary hydraulic fracturing (Fig. 15).

10.2. Fracture filling by satin spar

Fibrous gypsum on both sides of the median zone exhibits contrasting crystal morphologies and sizes to those in the median zone (Fig. 7), indicating a different formation mechanism (Bons and Montenari, 2005). The gypsum fibres with no signs of brittle failure and straining suggest a continuous rather than episodic growth more typically expected from a process involving pore fluid pressure build-up and release (Koehn et al., 2000; Barker et al., 2006). The question then arises regarding the origin of the fibrous habit of gypsum.

Previous studies suggested that crystal morphology in mineral veins is closely associated with growth competition (Bons and Jessell, 1997; Means and Li, 2001; Wiltschko and Morse, 2001; Hilgers and Urai, 2002). A lack of growth competition results in fibrous crystals, which only occurs in limited spaces, especially in fractures or voids with width less than 10 μm , or even

completely closed (Hilgers and Urai, 2002). Moreover, laboratory and numerical simulation of polycrystal growth suggest that growth competition may be inhibited when the growth rate of crystals exceeds the opening rate of cracks (Hilgers et al., 2001; Means and Li, 2001). Hence, nucleation of fibrous crystals on interfaces between host rocks and walls of median zones appears to postdate the sealing of the initial hydraulic fractures by mosaic crystals, as discussed above.

Vein expansion and fibre growth requires continued gypsum precipitation from supersaturated fluids (Cobbold and Rodrigues, 2007). Advective porous flow is unlikely to carry nutrient for the fibres due to the low-permeability bulk rock, especially when hydraulic fractures became sealed. Diffusion, driven by concentration gradient, could then be responsible for nutrient transport to satin spars (Fisher and Brantley, 1992; Bons et al., 2012; Rustichelli et al., 2016). Moreover, the much greater length of fibres than the width of median zones requires a vast amount of solution, which is unlikely to be transported by fluid flow in the bulk rock except through fractures. Hence, the continuous growth of fibres is attributed to diffusion of gypsum in the sediment pore network that is not necessarily accompanied by fluid flow and vein re-opening.

10.3. Timing and Phases of Veins

Gypsum in the subsurface readily dehydrates and converts to anhydrite when the ambient temperature rises up to 50-60°C (Testa and Lugli, 2000). Satin spar veins, which are considered to be filled with secondary gypsum, are suggested to occur at a relative shallow depth and a low ambient temperature. Coupled with the subsidence history of the Mercia Mudstone Group in the BCB (Kamerling, 1979), the development of veins is constrained to occur during the last uplift stage of the basin evolution. The diagenetic regenerated gypsum is likely to have resulted from

436 hydration of anhydrite when the evaporite beds were uplifted shallow enough that they entered
437 the telogenetic zone and came into contact with low salinity meteoric waters. However, based on
438 the crack-seal texture within the median zones of fractures, and precipitation of gypsum upon
439 faults moving in response to basin inversion, we suggest that the initiation of veins was not
440 triggered by the gypsum-anhydrite transition but by fluid overpressure. Later widening,
441 propagation, and linking likely owe to swelling related to anhydrite hydration.

442 The initial opening of the veins is interpreted to be the result of hydraulic fracturing due to
443 overpressure developed during the tectonic compression during basin inversion (c.f. Cosgrave,
444 2001), and help infer the timing of the veins to be broadly connected to the last inversion episode.
445 The fault veins that developed within the fault zones of the reactivated faults (Figs 10-13),
446 possibly suggest that some of the gypsum-rich fluids were transported along those faults during
447 fault dilation possibly as a result of seismic pumping behavior (Sibson et al., 1975).

448 As evident from the widely observed obliquity of fibres with respect to vein walls, the satin spar
449 veins are interpreted to be hybrid veins. Given the geometric patterns and lack of any systematic
450 cross-cutting relationships between differently oriented veins in the Keuper Marl, we infer a
451 small effective differential stress ($<4T$) at this time of vein initiation (Fig. 16). Such a stress field
452 is consistent with the generation of anastomosing fracture networks with frequent fracture
453 abutting and branching. However, we interpret the clear cross-cutting relationship between the
454 two sets of veins in the Tea Green Marl to mean at least two phases of fracturing.

455 Fault reactivation in the study area and adjacent areas of the Bristol Channel Basin is commonly
456 marked by slickenfibres with steps facing up-dip (Figs 10 and 13) (also Glen et al., 2005). The
457 two sets of fibre lineations in the median zone and on surfaces of fault vein possibly indicate a

minimum of two phases of fault reactivation. This interpretation is justified because such lineations only reveal the last slip event, and lineation for earlier slips could have been obscured or obliterated (Fossen, 2016). However, the pure, curved fibres in the fault veins (Figs 12C, 13B), which exhibit significantly different crystal morphology from the lineations, are likely to have formed during the inactivate period of the faults on the premise that mineral fibres could only nucleated in limited-closed spaces (Hilgers and Urai, 2002).

An important clue for the timing of the satin spar veins is that the folds in the Tea Green Marl are cut by the predominant sub-horizontal veins (Fig. 9F), suggesting the veins postdate the folding. Given the inferred timing of fault reactivation and buttress folding from late Oligocene to Miocene (Engelder and Peacock, 2001; Glen et al., 2005) as constraints, we infer that the satin spar veins formed during the Miocene or later.

10.4. Summary of Vein Genesis

Based on field and petrographic observations, a generic model is introduced to explain the dynamic process of the formation and growth of satin spar veins in mudstones. Initially, numerous discrete hydraulic fractures are generated in low-permeability mudstones due to overpressure, itself caused by inversion-related compression. Injection of sulphate-rich waters into fractures, including both the pre-existing and newly formed fractures, leads to rapid precipitation of equant, alabastrine gypsum on fracture walls as a result of the dramatic drop in fluid pressure, and healing of fractures. Due to the drop in fracture permeability, pore pressure could rise again, leading to vein reopening at vein-wall interfaces. This is accompanied with wall-parallel host rock bands detached from wall rocks. Such a process could occur repeatedly, producing a blocky, crack-seal texture in the median zone. After the cessation of fault

480 reactivations, pore pressure was not elevated so high as to reopen the healed veins. At this stage,
481 satin spars, which are fed by nutrient through diffusion, start to nucleate on the walls of the
482 blocky veins and grow continuously without further fracturing. This diffusion was driven by the
483 relative thermodynamic stability of gypsum at shallow depths.

484 **11. Conclusions**

485 (1) The satin spar veins initiated as natural hydraulic fractures or reactivated fractures in the low-
486 permeability marls of the Triassic Mercia Mudstone as a result of overpressure during basin
487 inversion.

488 (2) The satin spar veins exhibit characteristic features of antitaxial growth, but the blocky median
489 zone contains multiple bands of host rock inclusions and equant alabastrine gypsum, indicating
490 an origin comprising crack-seal events.

491 (3) Satin spar veins filling reactivated faults contain fibre lineations in the median zone and on
492 vein surfaces, indicating at least two phases of fault slip.

493 (4) The cross-cutting relationships between satin spar veins and other structures suggest the
494 formation timing to be Miocene.

495 (5) Fibre growth in satin spar veins was continuous and did not re-open veins; this later phase of
496 vein growth postdates initial hydrofracturing and sealing, and resulted from diffusion during the
497 anhydrite–gypsum transition.

(6) The satin spar veins of the Mercia Mudstone in the study area constitute an ideal analogue to subsurface hydraulic fracture systems in mudstone. However, their expansion owes to later diagenesis, which widened fractures and increased their connectivity.

Acknowledgements

This research is funded by Shell International Exploration and Production B.V. We thank Jon Wells for sample preparation, and Rick Allmendinger for providing Stereonet 9 software. We also thank Bruce Levell, Steve Hesselbo and Micha Ruhl for beneficial discussions. William Dunne is thanked for editorial handling of this manuscript. The thoughtful comments and constructive suggestions by the editor, Paul Bons and Brent Couzens-Schultz greatly improved the quality of this paper.

References

- Arvidson, R., Squyres, S., Bell, J., Catalano, J., Clark, B., Crumpler, L., De Souza, P., Fairén, A., Farrand, W., and Fox, V., 2014. Ancient aqueous environments at Endeavour crater, Mars. *Science* 343, 1248097.
- Barker, S. L., Cox, S. F., Eggins, S. M., and Gagan, M. K., 2006. Microchemical evidence for episodic growth of antitaxial veins during fracture-controlled fluid flow. *Earth and Planetary Science Letters* 250, 331-344.
- Barker, A. J., 2013. *Introduction to metamorphic textures and microstructures*. Routledge.
- Bons, P. D., and Jessell, M. W., 1997. Experimental simulation of the formation of fibrous veins by localised dissolution-precipitation creep. *Mineralogical Magazine* 61, 53-63.
- Bons, P. D., 2000. The formation of veins and their microstructures. *Journal of the Virtual Explorer* 2, 12.

520 Bons, P., 2001. Development of crystal morphology during unitaxial growth in a progressively
521 widening vein: I. The numerical model. *Journal of Structural Geology* 23, 865-872.

522 Bons, P. D., and Montenari, M., 2005. The formation of antitaxial calcite veins with well-
523 developed fibres, Oppaminda Creek, South Australia. *Journal of Structural Geology* 27,
524 231-248.

525 Bons, P. D., Elburg, M. A., and Gomez-Rivas, E., 2012. A review of the formation of tectonic
526 veins and their microstructures. *Journal of Structural Geology* 43, 33-62.

527 Brooks, M., Trayner, P., and Trimble, T., 1988. Mesozoic reactivation of Variscan thrusting in
528 the Bristol Channel area, UK. *Journal of the Geological Society* 145, 439-444.

529 Chadwick, R., 1986. Extension tectonics in the Wessex Basin, southern England. *Journal of the*
530 *Geological Society* 143, 465-488.

531 Cobbold, P. R., and Rodrigues, N., 2007. Seepage forces, important factors in the formation of
532 horizontal hydraulic fractures and bedding-parallel fibrous veins (beef and cone-in-cone).
533 *Geofluids* 7, 313-322.

534 Cobbold, P. R., Zanella, A., Rodrigues, N., and Løseth, H., 2013. Bedding-parallel fibrous veins
535 (beef and cone-in-cone): worldwide occurrence and possible significance in terms of
536 fluid overpressure, hydrocarbon generation and mineralization. *Marine and Petroleum*
537 *Geology*, 43, 1-20.

538 Cosgrove, J., 1993. The interplay between fluids, folds and thrusts during the deformation of a
539 sedimentary succession. *Journal of Structural Geology* 15, 491-500.

540 Cosgrove, J., 1995. The expression of hydraulic fracturing in rocks and sediments. *Geological*
541 *Society, London, Special Publications* 92, 187-196.

542 Cosgrove, J. W., 2001. Hydraulic fracturing during the formation and deformation of a basin: A
543 factor in the dewatering of low-permeability sediments. AAPG Bulletin 85, 737-748.

544 Couzens-Schultz, B. A., and Azbel, K., 2014. Predicting pore pressure in active fold–thrust
545 systems: An empirical model for the deepwater Sabah foldbelt. Journal of Structural
546 Geology 69, 465-480.

547 Coward, M., 1995. Structural and tectonic setting of the Permo-Triassic basins of northwest
548 Europe. Geological Society, London, Special Publications 91, 7-39.

549 Cox, S., and Etheridge, M., 1983. Crack-seal fibre growth mechanisms and their significance in
550 the development of oriented layer silicate microstructures. Tectonophysics 92, 147-170.

551 Dart, C. J., McClay, K., and Hollings, P. N., 1995. 3D analysis of inverted extensional fault
552 systems, southern Bristol Channel basin, UK. Geological Society, London, Special
553 Publications 88, 393-413.

554 De Meer, S., and Spiers, C.J., 1995. Creep of wet gypsum aggregates under hydrostatic loading
555 conditions. Tectonophysics 245: 171-183.

556 De Meer, S., and Spiers, C.J., 1997. Uniaxial compaction creep of wet gypsum aggregates.
557 Journal of Geophysical Research: Solid Earth 102: 875-891.

558 Donato, J., 1988. Possible Variscan thrusting beneath the Somerton anticline, Somerset. Journal of the Geological
559 Society 145, 431-438.

560 Durney, D. W., and Ramsay, J., 1973. Incremental strains measured by syntectonic crystal
561 growths. Gravity and tectonics 67, 96.

562 Engelder, T., and Peacock, D. C., 2001. Joint development normal to regional compression
563 during flexural-flow folding: the Lillstock buttress anticline, Somerset, England. Journal
564 of Structural Geology 23, 259-277.

565 Fisher, D. M., and Brantley, S. L., 1992. Models of quartz overgrowth and vein formation:
566 deformation and episodic fluid flow in an ancient subduction zone. *Journal of*
567 *Geophysical Research: Solid Earth* 97, 20043-20061.

568 Fossen, H., 2016. *Structural geology*. Cambridge University Press.

569 Gale, J. F., and Holder, J., 2010. Natural fractures in some US shales and their importance for
570 gas production. *Geological Society, London, Petroleum Geology Conference Series* 7,
571 1131-1140.

572 Glen, R., Hancock, P., and Whittaker, A., 2005. Basin inversion by distributed deformation: the
573 southern margin of the Bristol Channel Basin, England. *Journal of Structural Geology* 27,
574 2113-2134.

575 Gustavson, T. C., Hovorka, S. D., and Dutton, A. R., 1994. Origin of satin spar veins in evaporite
576 basins. *Journal of Sedimentary Research* 64, 88-94.

577 Hilgers, C., Koehn, D., Bons, P., and Urai, J., 2001. Development of crystal morphology during
578 uniaxial growth in a progressively widening vein: II. Numerical simulations of the
579 evolution of antiaxial fibrous veins. *Journal of Structural Geology* 23, 873-885.

580 Hilgers, C., and Urai, J. L., 2002. Microstructural observations on natural syntectonic fibrous
581 veins: implications for the growth process. *Tectonophysics* 352, 257-274.

582 Hobbs, P., Hallam, J., Forster, A., Entwisle, D., Jones, L., Cripps, A., Northmore, K., Self, S.,
583 and Meakin, J., 2002. *Engineering geology of British rocks and soils: Mudstones of the*
584 *Mercia Mudstone Group*. British Geological Survey.

585 Holford, S. P., Turner, J. P., and Green, P. F., 2005. Reconstructing the Mesozoic–Cenozoic
586 exhumation history of the Irish Sea basin system using apatite fission track analysis and

587 vitrinite reflectance data. Geological Society, London, Petroleum Geology Conference
588 series 6, 1095-1107.

589 Holloway, S., and Chadwick, R., 1986. The Sticklepath-Lustleigh fault zone: Tertiary sinistral
590 reactivation of a Variscan dextral strike-slip fault. *Journal of the Geological Society* 143,
591 447-452.

592 Howard, A., Warrington, G., Ambrose, K., and Rees, J., 2008. A formational framework for the
593 Mercia Mudstone Group (Triassic) of England and Wales. British Geological Survey.

594 Ingram, G., Chisholm, T., Grant, C., Hedlund, C., Stuart-Smith, P., and Teasdale, J., 2004.
595 Deepwater North West Borneo: hydrocarbon accumulation in an active fold and thrust
596 belt. *Marine and Petroleum Geology* 21, 879-887.

597 Kamerling, P., 1979. The geology and hydrocarbon habitat of the Bristol Channel Basin. *Journal*
598 *of Petroleum Geology* 2, 75-93.

599 Keary, P., and Vine, F., 1990. *Global Tectonics*. Blackwell, Oxford.

600 Kelly, P., Peacock, D., Sanderson, D., and McGurk, A., 1999. Selective reverse-reactivation of
601 normal faults, and deformation around reverse-reactivated faults in the Mesozoic of the
602 Somerset coast. *Journal of Structural Geology* 21, 493-509.

603 Koehn, D., Hilgers, C., Bons, P. D., and Passchier, C. W., 2000. Numerical simulation of fibre
604 growth in antitaxial strain fringes. *Journal of Structural Geology* 22, 1311-1324.

605 Laubach, S., Reed, R., Olson, J., Lander, R., and Bonnell, L., 2004. Coevolution of crack-seal
606 texture and fracture porosity in sedimentary rocks: cathodoluminescence observations of
607 regional fractures. *Journal of Structural Geology* 26, 967-982.

608 Luo, X., Wang, Z., Zhang, L., Yang, W., and Liu, L., 2007. Overpressure generation and
609 evolution in a compressional tectonic setting, the southern margin of Junggar Basin,
610 northwestern China. AAPG Bulletin 91, 1123-1139.

611 Machel, H. G., 1985. Fibrous gypsum and fibrous anhydrite in veins. Sedimentology 32, 443-454.

612 Mandl, G., 2005. Rock joints. Springer, Berlin.

613 Mauldon, M., Dunne, W., and Rohrbaugh, M., 2001. Circular scanlines and circular windows:
614 new tools for characterizing the geometry of fracture traces. Journal of Structural
615 Geology 23, 247-258.

616 Means, W., and Li, T., 2001. A laboratory simulation of fibrous veins: some first observations.
617 Journal of Structural Geology 23, 857-863.

618 Menpes, R. J., and Hillis, R. R., 1995. Quantification of Tertiary exhumation from sonic velocity
619 data, Celtic Sea/south-western approaches. Geological Society, London, Special
620 Publications 88, 191-207.

621 Miliorizos, M., and Ruffell, A., 1998. Kinematics of the Watchet-Cothelstone-Hatch fault system:
622 implications for the fault history of the Wessex basin and adjacent areas. Geological
623 Society, London, Special Publications 133, 311-330.

624 Mohamed El Tabakh, B., and Warren, J. K., 1998. Origin of fibrous gypsum in the Newark rift
625 basin, eastern North America. Journal of Sedimentary Research 68, 88-99.

626 Moragas, M., Martínez, C., Baqués, V., Playà, E., Travé, A., Alías, G., and Cantarero, I., 2013.
627 Diagenetic evolution of a fractured evaporite deposit (Vilobí Gypsum Unit, Miocene, NE
628 Spain). Geofluids 13, 180-193.

629 Murray, R., 1964. Origin and diagenesis of gypsum and anhydrite. Journal of Sedimentary
630 Research 34, 512-523.

631 Nachon, M., Clegg, S., Mangold, N., Schröder, S., Kah, L., Dromart, G., Ollila, A., Johnson, J.,
 632 Oehler, D., and Bridges, J., 2014. Calcium sulfate veins characterized by
 633 ChemCam/Curiosity at Gale crater, Mars. *Journal of Geophysical Research: Planets* 119,
 634 1991-2016.

635 Nemčok, M., Gayer, R., and Milorizos, M., 1995. Structural analysis of the inverted Bristol
 636 Channel Basin: implications for the geometry and timing of fracture porosity. *Geological*
 637 *Society, London, Special Publications* 88, 355-392.

638 Nichols, G., 2009. *Sedimentology and stratigraphy*. John Wiley & Sons.

639 Oliver, N. H., and Bons, P. D., 2001. Mechanisms of fluid flow and fluid–rock interaction in
 640 fossil metamorphic hydrothermal systems inferred from vein–wallrock patterns,
 641 geometry and microstructure. *Geofluids* 1, 137-162.

642 Passchier, C. W., and Trouw, R. A., 1996. *Microtectonics*. Springer, Berlin.

643 Peacock, D., and Sanderson, D., 1991. Displacements, segment linkage and relay ramps in
 644 normal fault zones. *Journal of Structural Geology* 13, 721-733.

645 Peacock, D., 1992. Effects of layering and anisotropy on fault geometry. *Journal of the*
 646 *Geological Society* 149, 793-802.

647 Peacock, D., 1994. Geometry and development of relay ramps in normal fault systems. *AAPG*
 648 *Bulletin* 78, 147-165.

649 Peacock, D., 1999. Deformation history and basin-controlling faults in the Mesozoic sedimentary
 650 rocks of the Somerset coast. *Proceedings of the Geologists' Association* 110, 41-52.

651 Philipp, S. L., 2008. Geometry and formation of gypsum veins in mudstones at Watchet,
 652 Somerset, SW England. *Geological Magazine* 145, 831-844.

653 Ramsay, J. G., 1980. The crack-seal mechanism of rock deformation. *Nature* 284, 135-139.

654 Rawnsley, K., Peacock, D., Rives, T., and Petit, J.-P., 1998. Joints in the Mesozoic sediments
655 around the Bristol Channel Basin. *Journal of Structural Geology* 20, 1641-1661.

656 Roberts, D., 1989. Basin inversion in and around the British Isles. Geological Society, London,
657 Special Publications 44, 131-150.

658 Ruffell, A., and Coward, M., 1992. Basement tectonics and their relationship to Mesozoic
659 megasequences in the Celtic Seas and Bristol Channel area. Geological Society, London,
660 Special Publications 62, 385-394.

661 Ruffell, A., and Shelton, R., 1999. The control of sedimentary facies by climate during phases of
662 crustal extension: examples from the Triassic of onshore and offshore England and
663 Northern Ireland. *Journal of the Geological Society* 156, 779-789.

664 Rustichelli, A., Di Celma, C., Tondi, E., Baud, P., and Vinciguerra, S., 2016. Fibrous gypsum
665 veins as diffuse features and within fault zones: the case study of the Pisco Basin (Ica
666 desert, southern Peru). *Journal of the Geological Society* 173, 405-418.

667 Shearman, D., Mossop, G., Dunsmore, H., and Martin, M., 1972. Origin of gypsum veins by
668 hydraulic fracture. *Institution of Mining and Metallurgy Transaction, Section B: Applied*
669 *Earth Science* 81, 149-155.

670 Sheorey, P.R., 1994. A theory for *in situ* stresses in isotropic and transversely isotropic rock.
671 *International Journal of Rock Mechanics and Mining Sciences* 31 (1), 23-34.

672 Sibson, R., Moore, J. M. M., and Rankin, A., 1975. Seismic pumping—a hydrothermal fluid
673 transport mechanism: *Journal of the Geological Society* 131, 653-659.

674 Squyres, S. W., Arvidson, R. E., Bell, J., Calef, F., Clark, B., Cohen, B., Crumpler, L., De Souza,
675 P., Farrand, W., and Gellert, R., 2012. Ancient impact and aqueous processes at
676 Endeavour Crater, Mars. *Science* 336, 570-576.

677 Talbot, M., Holm, K., and Williams, M., 1994. Sedimentation in low-gradient desert margin
678 systems: A comparison of the Late Triassic of northwest Somerset (England) and the late
679 Quaternary of east-central Australia. Geological Society of America Special Papers 289,
680 97-117.

681 Teixell, A., Durney, D. W., and Arboleya, M.-L., 2000. Stress and fluid control on décollement
682 within competent limestone. Journal of Structural Geology 22, 349-371.

683 Testa, G., and Lugli, S., 2000. Gypsum–anhydrite transformations in Messinian evaporites of
684 central Tuscany (Italy). Sedimentary Geology 130, 249-268.

685 Tucker, M., 1977. The marginal Triassic deposits of South Wales: continental facies and
686 palaeogeography. Geological Journal 12, 169-188.

687 Tucker, M. E., 2009. Sedimentary petrology: an introduction to the origin of sedimentary rocks.
688 John Wiley & Sons.

689 Van der Pluijm, B. A., 1984. An unusual ‘crack-seal’ vein geometry. Journal of structural
690 geology 6, 593-597.

691 Van Hoorn, B., 1987. The south Celtic Sea/Bristol Channel Basin: origin, deformation and
692 inversion history. Tectonophysics 137, 309-334.

693 Virgo, S., Abe, S., and Urai, J.I., 2014. The evolution of crack seal vein and fracture networks in
694 an evolving stress field: insights from discrete element models of fracture sealing. Journal
695 of Geophysical Research: Solid Earth 119, 8708-8727.

696 Warren, J. K., 2006. Evaporites: sediments, resources and hydrocarbons. Springer Science &
697 Business Media.

698 Warrington, G., Cope, J., and Ivimey-Cook, H., 1994. St Audrie's Bay, Somerset, England: a
699 candidate global stratotype section and point for the base of the Jurassic system.
700 Geological Magazine 131, 191-200.

701 Whittaker, A., 1972. The Watchet Fault—a post Liassic transcurrent reverse fault. Bulletin of the
702 Geological Survey 41, 75-80.

703 Whittaker, A., and Green, G. W., 1983. Geology of the country around Weston-super-Mare. HM
704 Stationery Office.

705 Wiltschko, D. V., and Morse, J. W., 2001. Crystallization pressure versus “crack seal” as the
706 mechanism for banded veins. Geology 29, 79-82.

Fig. 1. Geological map of the study area (A) on the Warren Bay; and (B) cross-section along A-A' line. Locations for Figs. 3A, 3C, 4A-B, 5A-D, 5E-F, 10-12, and 13A are shown in Fig. 1A. BCB, Bristol Channel Basin. Vein (black) and bedding (bold) orientation data plotted on stereonet as great circles (lower hemisphere). See vein orientation data in Table S1 (supplementary material). Geological map is modified from Dart et al. (1995) and Glen et al. (2005).

Fig. 2. Stratigraphic column of the Triassic and Early Jurassic of the BCB. Adapted from Hobbs et al. (2002).

Fig. 3. Outcrop photographs showing sandstone dykes in the Keuper Marl. (A) A normal fault cross-cuts a sandstone dyke (yellow-dotted line). The enlarged box shows a gypsum nodule being cross-cut by the sandstone dyke. The arrows show the nodular gypsum horizons as markers for bedding correlation. See location in Fig. 1A. (B) A steeply dipping sandstone dyke cross-cuts multiple nodular gypsum horizons. The enlarged area shows the sub-horizontal satin spar veins cross-cutting the sandstone dyke. (C) A curved sandstone dyke cross-cut by sub-horizontal satin spar veins. HRF, host rock fragment. Hammer is 30 cm long. See location in Fig. 1A. (D) Sketch of Fig. 3C.

Fig. 4. Outcrop photographs showing inversion-related structures. (A) Buttress folding of the layers of the TGM in the hanging wall of the Helwell Bay Fault. The faults are highlighted by red lines. 1, gently inclined satin spar veins cross-cut folded layers of the TGM. 2, bedding-parallel veins in the KM cross-cut by the Helwell Bay Fault. (B) Detachment folds of the layers of the Blue Lias Formation above weak layers of the TGM with abundant nodular gypsum. Note that the fold is modified by some reverse faults. See location in Fig. 1A. BL, Blue Lias

Formation. HBF, Helwell Bay Fault. KM, Keuper Marl. TGM, Tea Green Marl. NG, nodular gypsum.

Fig. 5. Outcrop photographs showing satin spar veins in the Keuper Marl (A-D) and the Tea Green Marl (E-F). (A) Anastomosing satin spar vein network. (B) Closely spaced sub-horizontal satin spar veins. Notebook is 15 cm long. (C) Vein networks showing three major preferred orientations (normal to arrows). The circle shows the circular window for vein orientation measurement. Tape measure is 1 m long. (D) A short vein with tapering tips. (E) Slabs of red steep veins exposed in the cliffs. Note the white vein cross-cuts the red veins. Note book is 20 cm in length. (F) Sigmoidal shaped red, intact veins in gently dipping beds. See locations in Fig. 1A.

Fig. 6. En echelon veins in the outcrop (A-B) and thin sections (C-H). (A) A sub-horizontal vein in the Keuper Marl with host rock fragments which are oblique to vein walls. UTM position: Northing 5670230, Easting 476433, Zone 30U. (B) Sigmoidal shaped veins in the Tea Green Marl. UTM position: Northing 5670064, Easting 475911, Zone 30U. (C) A set of small en echelon veins in red marls. (D) The coalescence of two parallel veins, leaving the host rock fragment trapped between the vein tips. (E) A vein with impurities of oblique host rock inclusions. Samples in Fig. 6C-E are from the same site as the vein in Fig. 6A. (F) Sketch of Fig. 6E. (G) A sub-horizontal vein with four wall-oblique host rock fragments. UTM position: Northing 5670116, Easting 476016, Zone 30U. (H) Sketch of Fig. 6G.

Fig. 7. Outcrop photographs (A-B) and photomicrographs (C-F) showing texture and composition of satin spar veins. (A) A sub-horizontal satin spar vein in the Keuper Marl. Note that the fibres are oblique to vein walls. Camera diameter is 5.2 cm. (B) A sub-horizontal vein

consisting of a dark median zone and two fibrous zones on different sides of the median zone. Pen head is 5 cm. (C) The blocky median zone of a representative satin spar vein, consisting of multiple thin bands of host rock inclusions and numerous interlocking alabastrine gypsum crystals. (D) Sketch of Fig. 7C. (E) A curved median zone of a satin spar vein. Note that the host rock inclusion bands are parallel to the margin of the median zone. (F) Parallel aligned fibres on one side of the median zone. The fibres show rather constant width and smooth crystal boundaries.

Fig. 8. Outcrop photographs (A-D) and photomicrographs (E) showing the behavior of vein branching. (A) A sub-horizontal vein splits into a sub-horizontal branch and an inclined branch. Note that the median zone (highlighted by arrows) is retained in the sub-horizontal branch. (B) Branching in both the upper and lower parts in a thick vein. (C) Coalescence of vein branches, resulting a connected vein network. (D) A thick vein split into three branches. (E) Multiple branches for a single satin spar vein. Cross polars.

Fig. 9. Intersection of differently oriented satin spar veins in the Keuper Marl (A-E) and the sub-horizontal veins in the folded layers in the Tea Green Marl (F). (A) Intersection of veins of set K-1 and sub-horizontal veins of set K-3. Note that the veins do not cross-cut and instead, form an anastomosing network. (B) Coalescence of curved satin spar veins. (C) Coalescence of sub-horizontal veins with steeply dipping veins. The enlarged box shows the tapering tip of a sub-horizontal vein towards the steep vein. (D) Sub-horizontal veins with a steeply dipping step. (E) Steeply dipping veins formed as wing-cracks of thick sub-horizontal veins. Note the increase in vein aperture towards the sub-horizontal vein. (F) Curvy, sub-horizontal satin spar veins cross-cut the folded layers in the Tea Green Marl.

Fig. 10. Outcrop photograph showing a fault vein cross-cutting sub-horizontal veins in the bulk rock. UTM position: Northing 5670244, Easting 476500, Zone 30U. (A) The fault shows a reverse displacement. Note the sub-horizontal veins and nodular horizons (green-yellow arrows) as markers for bedding correlation. Tape measure is 1 m long. See location in Fig. 1A. (B) The plane of the fault vein with fibre lineations which are parallel to the striations in the wall rock in Fig. 10C. The dashed line mark lineation orientation. (D) Steps and depressions on the plane of the fault vein, which are interpreted to have been created during fault reverse slip.

Fig. 11. Outcrop photographs showing the fault vein filling the Helwell Bay Fault. UTM position: Northing 5670073, Easting 475929, Zone 30U. See location in Fig. 1A. (A) The fault vein cross-cuts the white satin spar vein (arrows). (B) Fibre lineations in the fault vein, indicating the last slip direction of the fault. (C) Dark striations on a sub-horizontal fault vein. Pen is 15 cm long. (D) Propagation of a horizontal gypsum vein (yellow arrow) along the plane of a normal fault. UTM position: Northing 5670154, Easting 476101, Zone 30U.

Fig. 12. (A) Outcrop photograph showing a thick fault vein filling a normal fault. UTM position: Northing 5670248, Easting 476536, Zone 30U. See location in Fig. 1A. (B) The fault vein consists of impure median zones of gypsum and host rock inclusions. The outer parts contains pure, curved gypsum fibres. (C) Curved gypsum fibres with increased plunge towards the vein wall. See location in the box in Fig. 12B.

Fig. 13. (A) A fault with a reverse displacement, which is marked by the green siltstone layer (arrow). UTM position: Northing 5670231, Easting 476444, Zone 30U. See location in Fig. 1A. (B) The fault vein filling the fault in Fig. 13A. The dashed lines highlight the fibre traces. (C)

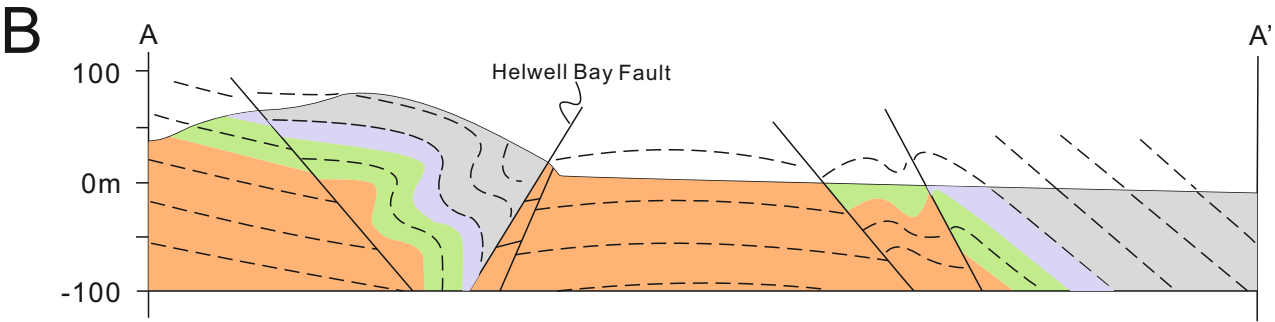
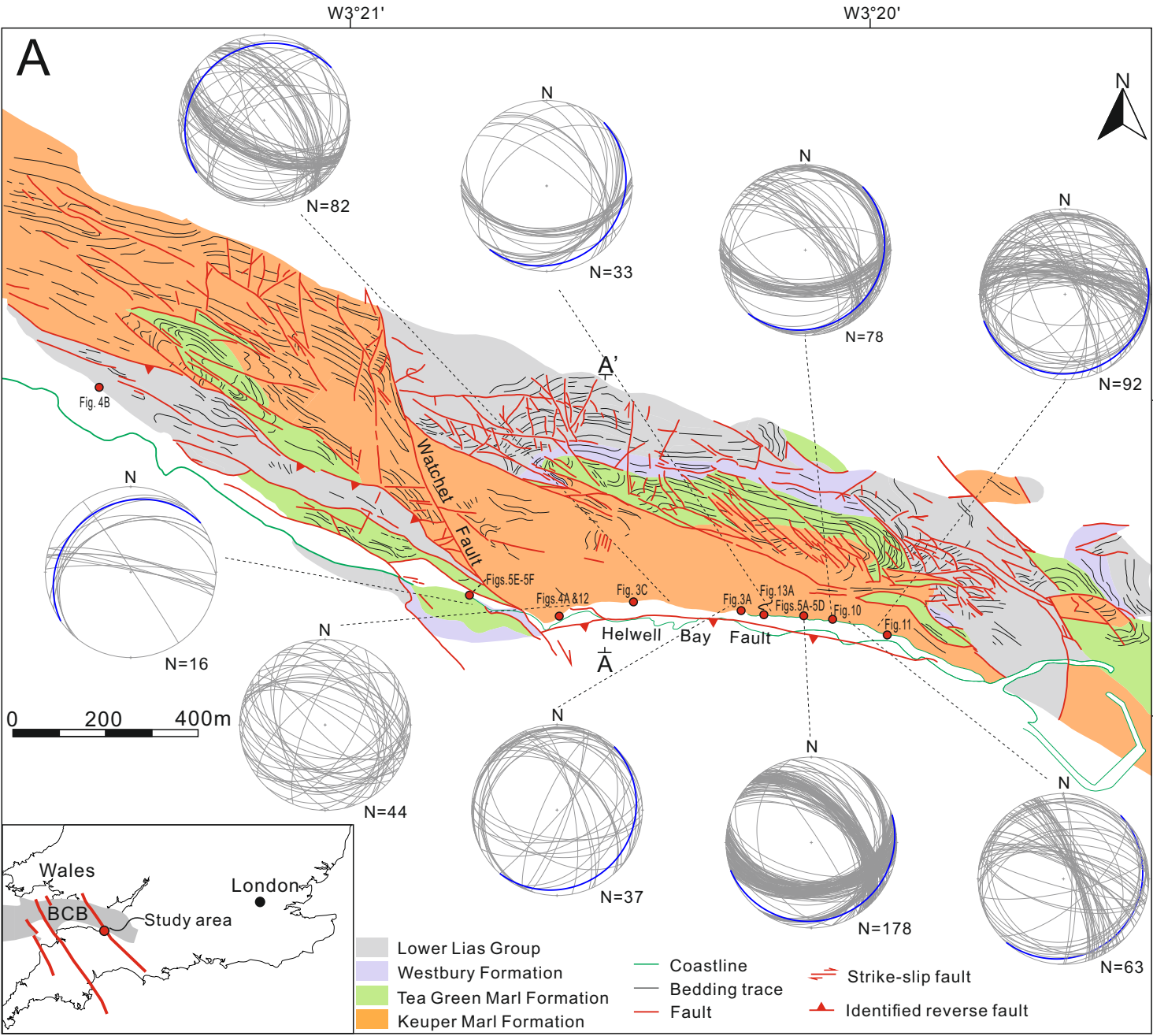
Fibre lineations on the plane of the fault vein. Note the steps that indicate the reverse motion. (D)
Sketch illustrating the representative textures of fault veins.

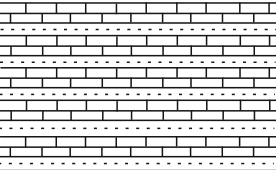
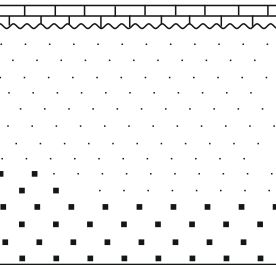
Fig. 14 Sketch illustrating repeated fault reactivation with fault vein-filling by gypsum. T1: The sediments were loaded with a maximum sub-horizontal compressive stress. T2: The faults were reactivated with reverse motions recorded by fibre lineations. T3: Pure gypsum fibres grew when the faults were inactive and fully sealed. T4: Fibre lineations were produced on the planes of fault veins during another phase of fault reactivation.


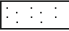

Fig. 15. Sketch illustrating the process of branching of satin spar veins. T1: Initial cracking. T2: Antitaxial growth of gypsum fibres. The fibres are gently inclined towards the left side of the figure because the resolved shear stress caused left-lateral relative motion of the vein walls. T3: Vein splitting during incremental widening of the vein. Note the bifurcation located in the fibrous zone rather than the median zone. The fibres in the thin branch are gently inclined towards the right side of the figure because its walls exhibit a right-lateral relative motion.

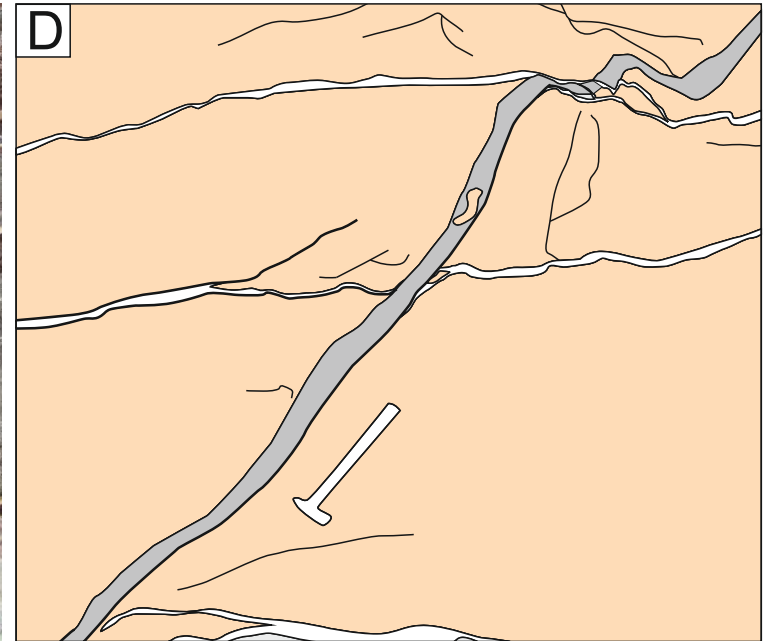
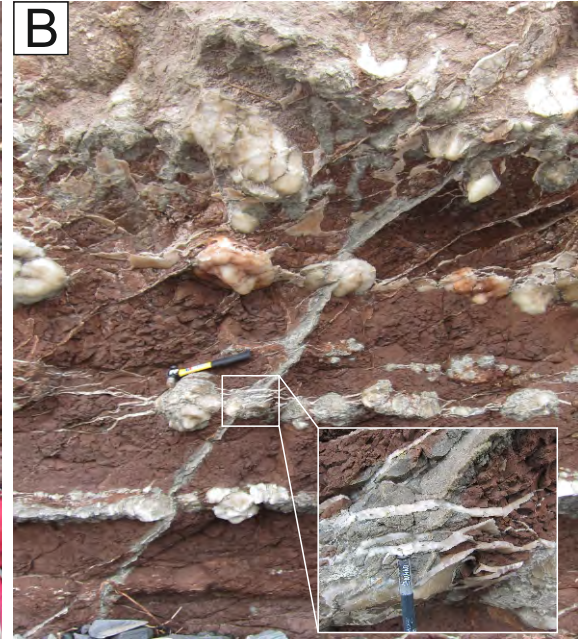
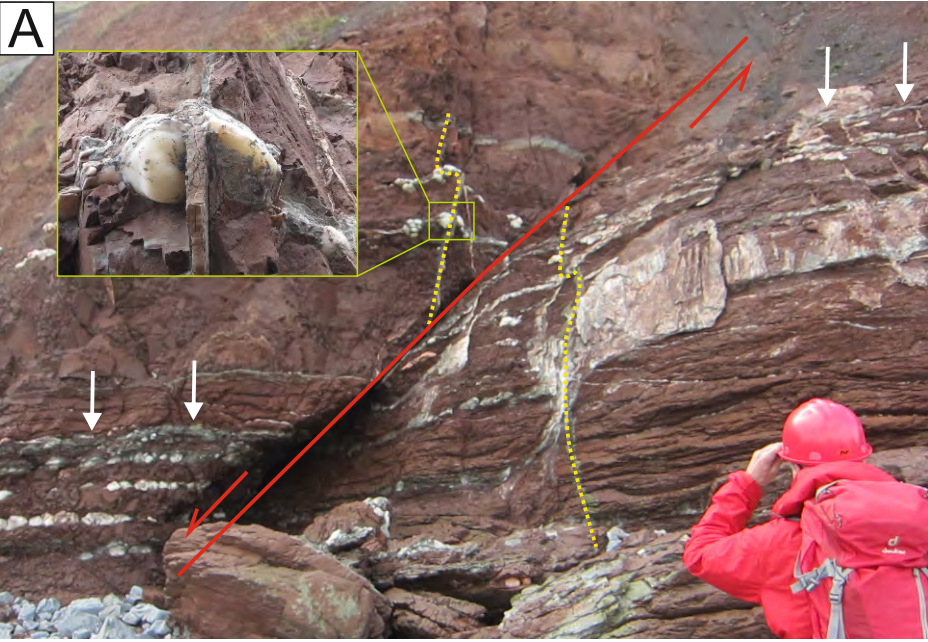
Fig. 16. (A) Subsidence curve for the Mercia Mudstone in the north Somerset region. Modified from Cosgrove (2001). Basin inversion is evident from fault reactivation. Vein generation is estimated to occur near surface with a horizontal maximum principal stress. (B) Navier-Coulomb-Griffith combined extensional and shear brittle failure envelope showing the stress states which cause extensional (I, II and III) and shear-extensional failure (IV). I-II all have differential stresses less than $4T$ (T , tensile strength). IV has a differential stress around $4T$. Stress diagram is modified from Cosgrove (1995). (C) Field observations of vein network that are compatible with the stress states illustrated in II-IV, indicating a low differential stress causing the formation of satin spar veins.

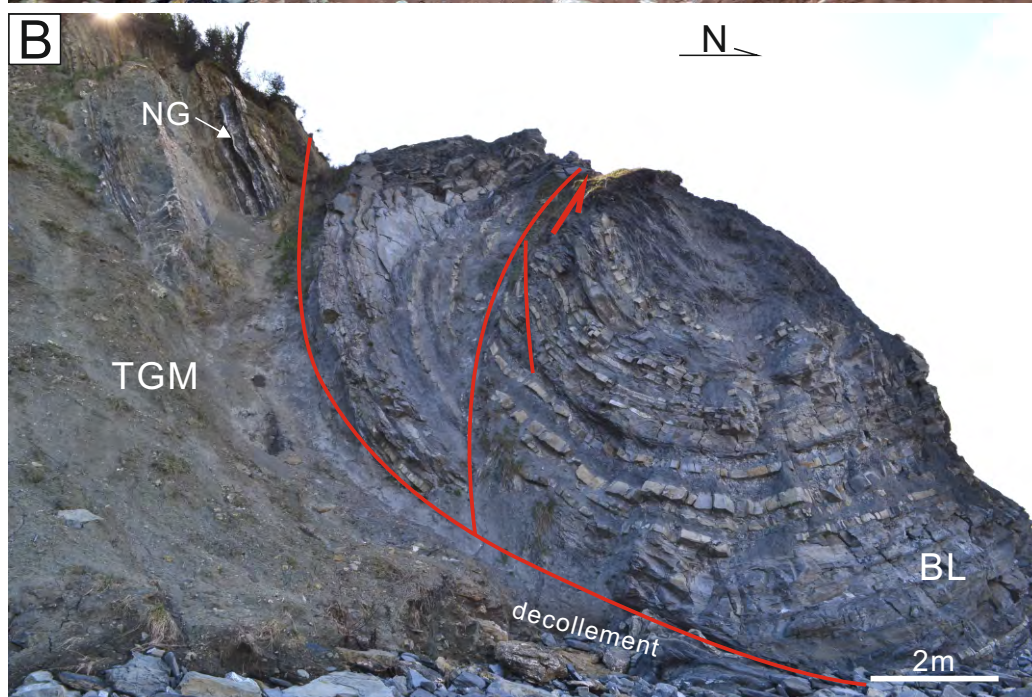
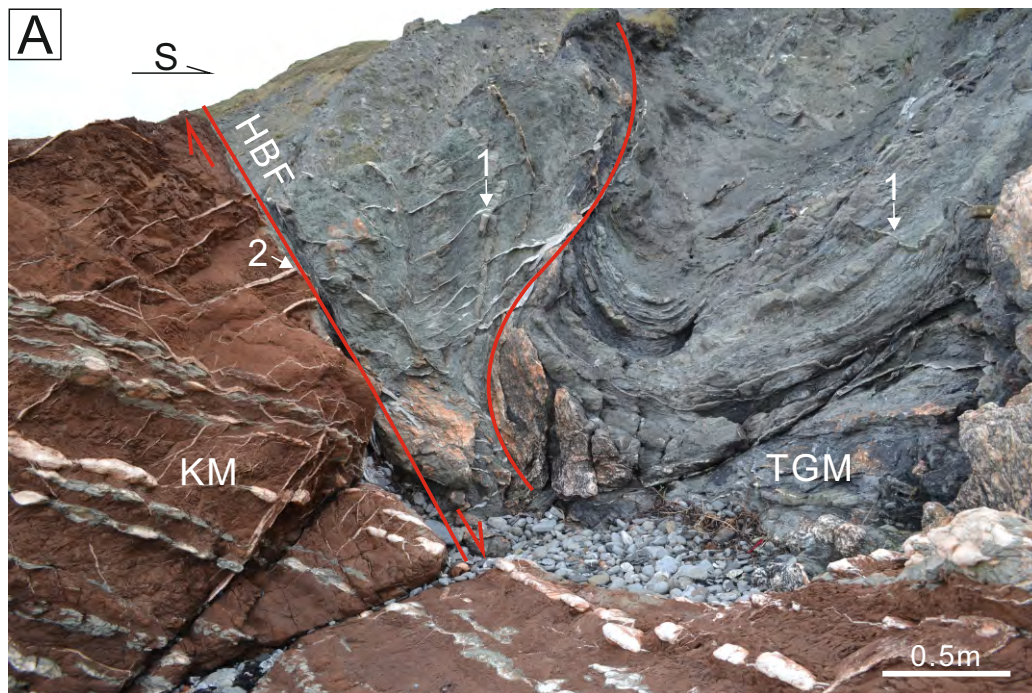
*Figure

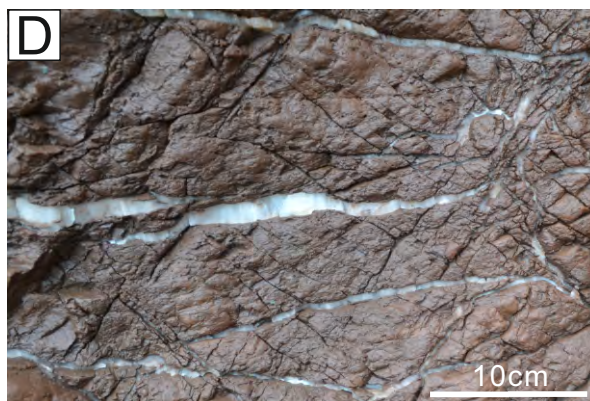
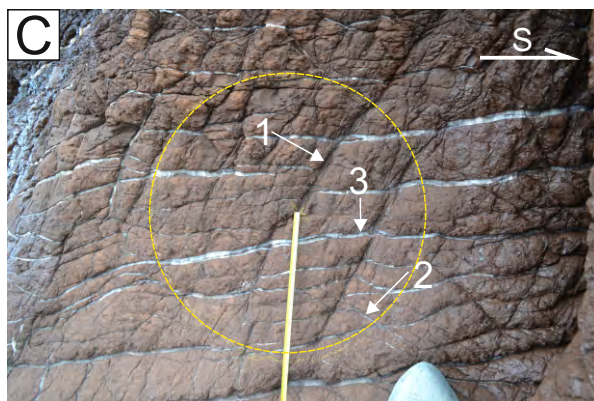
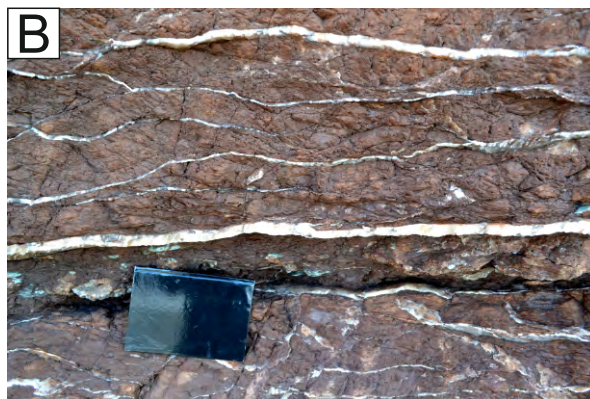


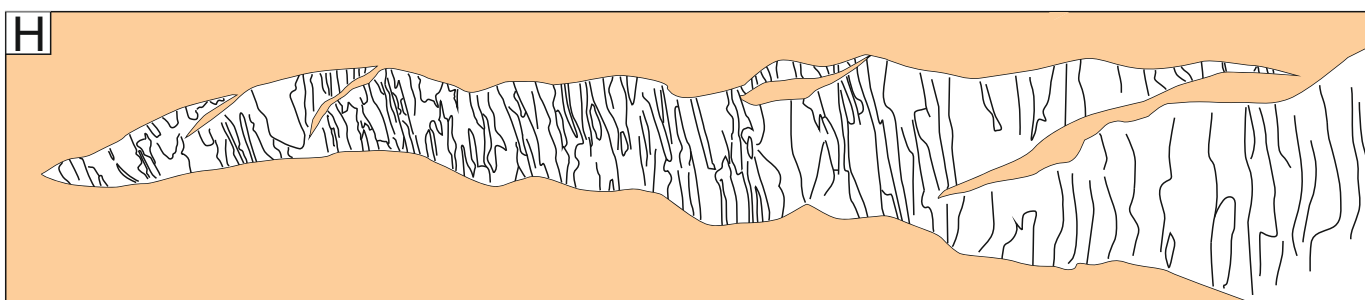
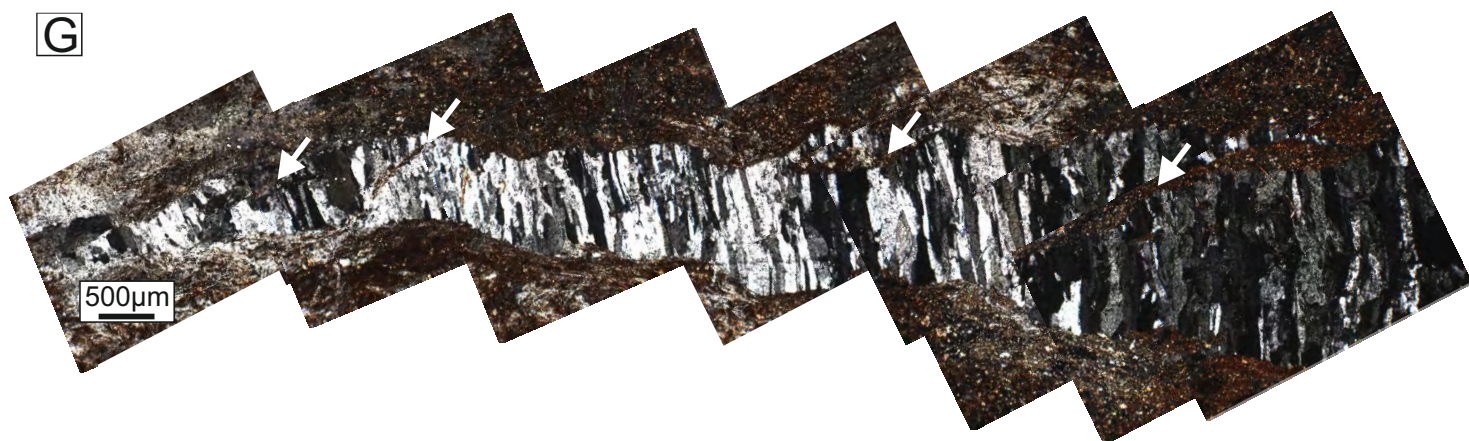
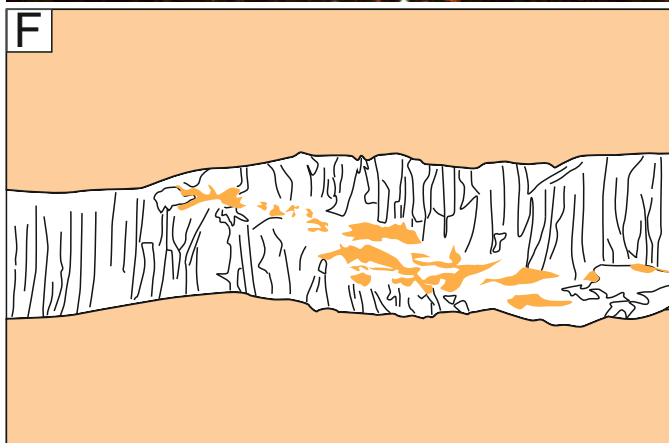
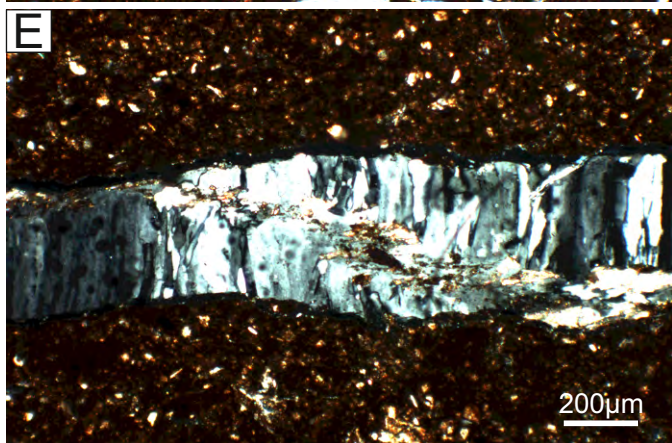
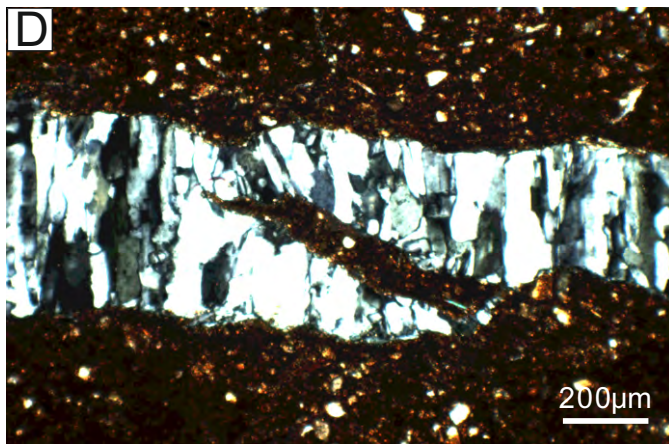
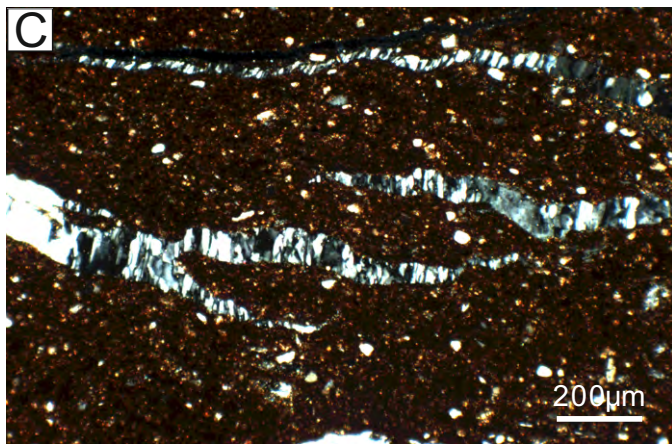
		AGE	LITHOLOGY	STRATIGRAPHY
JURASSIC	EARLY	TOARCIAN		LIAS GROUP
		PLIENSBACH		
		SINEMURIAN		BLUE LIAS
		HETTANGIAN		
TRIASSIC	LATE	NORIAN		PENARTH GROUP
				MERCIA MUDSTONE GROUP
	MID	LADINIAN		SHERWOOD SANDSTONE GROUP
		ANISIAN		
	E	SCYTHIAN		
PERMIAN				

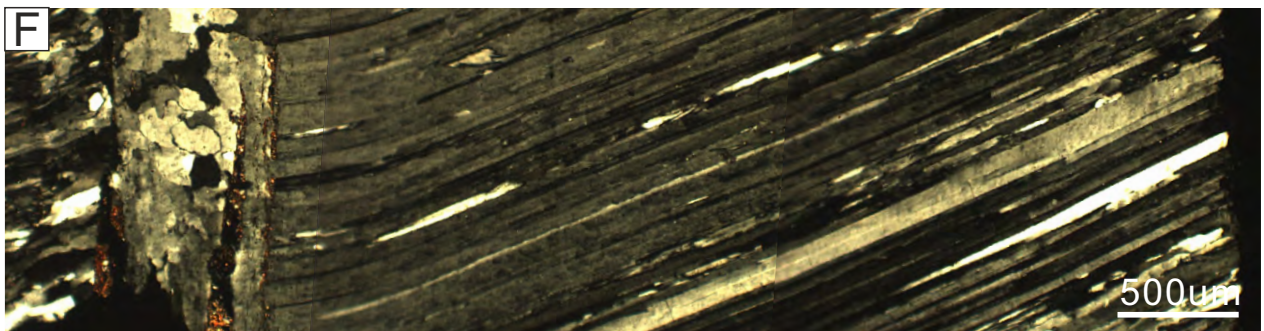
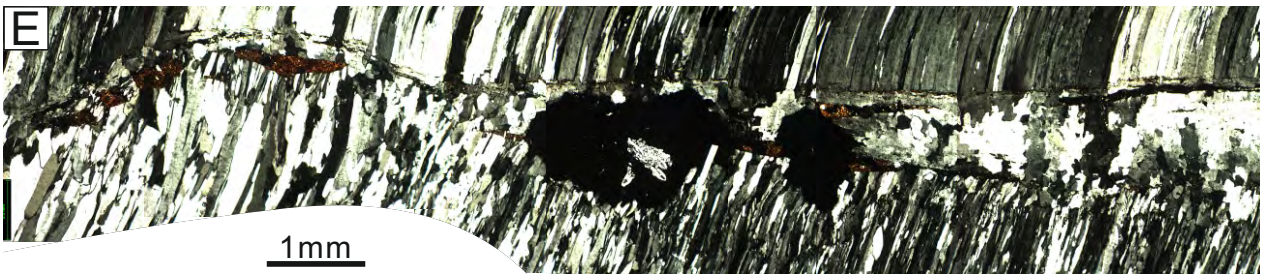
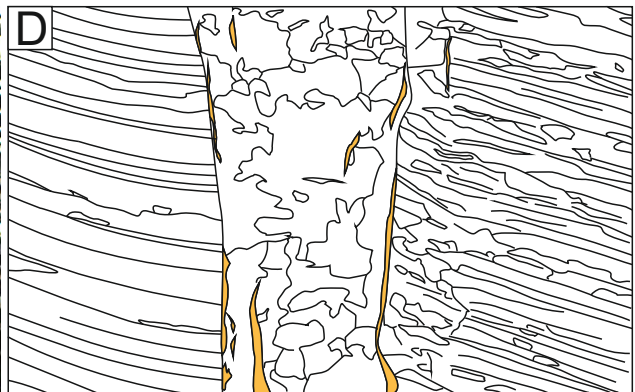
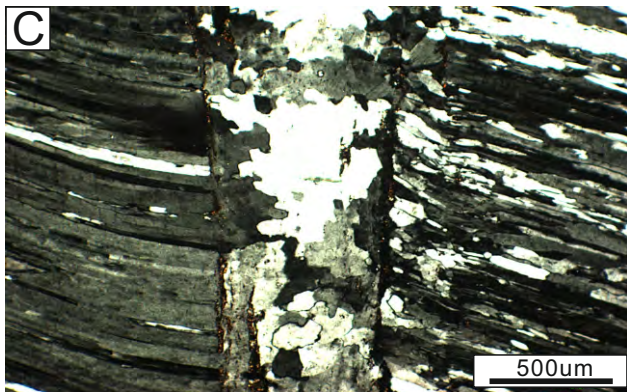
 Interbedded limestone and shale
  Mudstone
  Sandstone

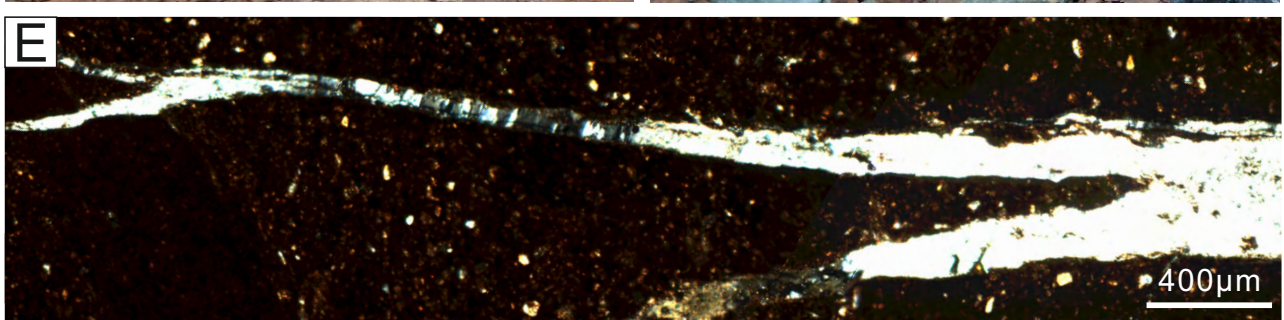


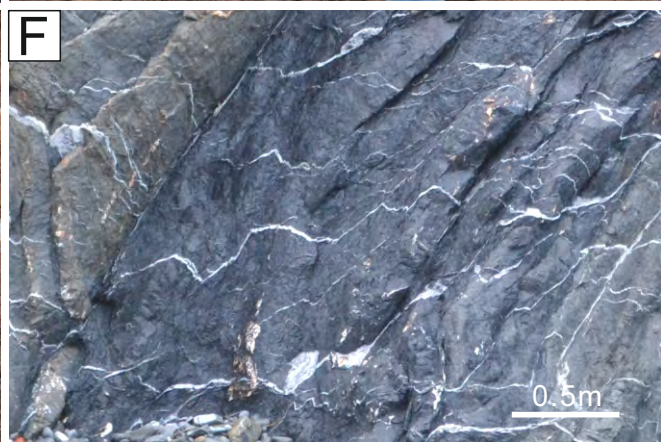
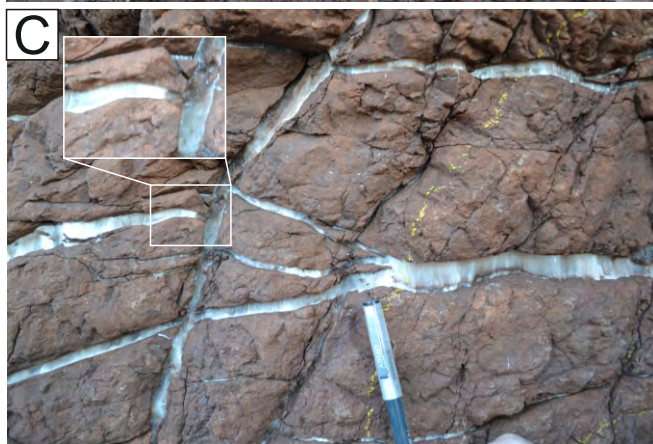
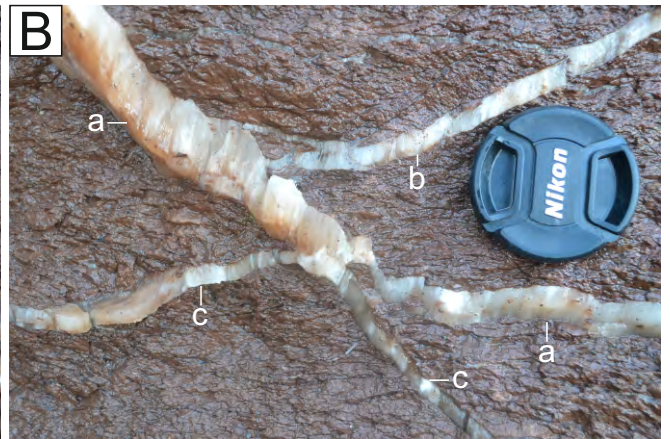
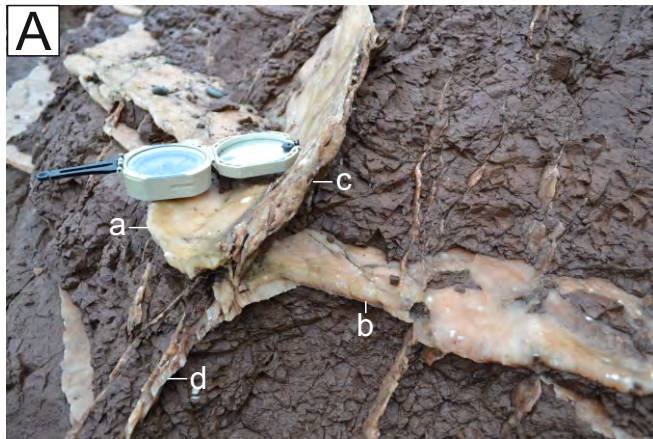


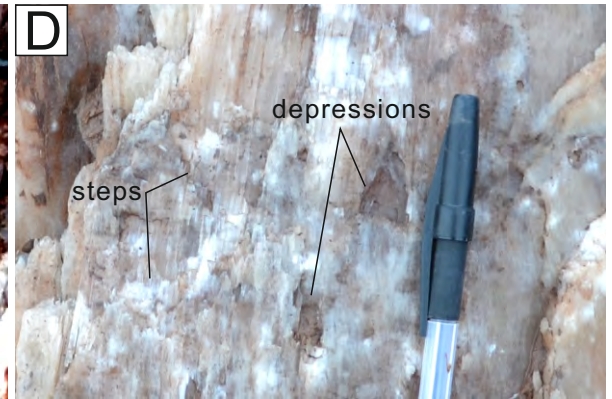
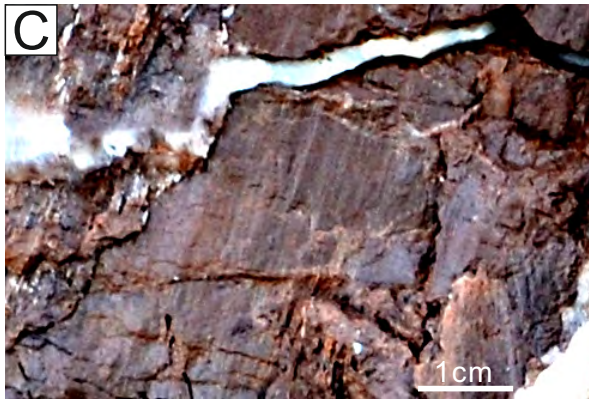
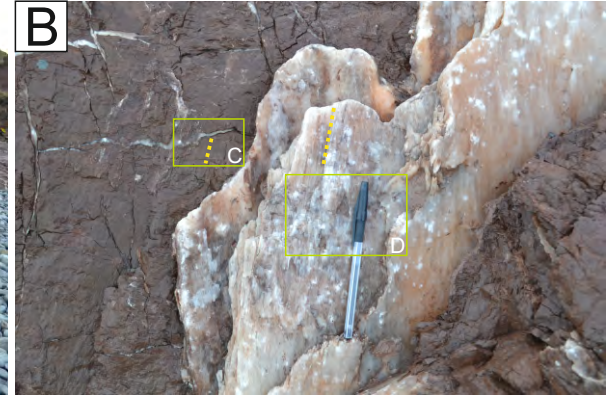


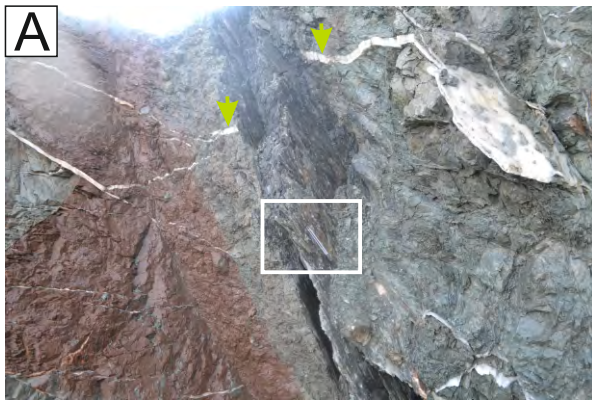


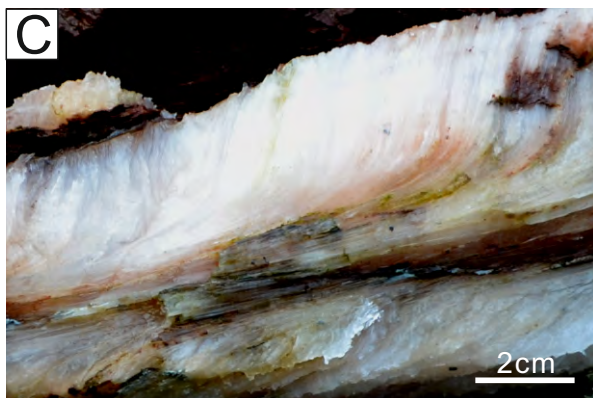


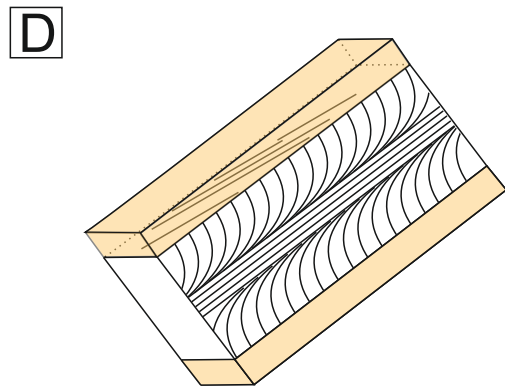
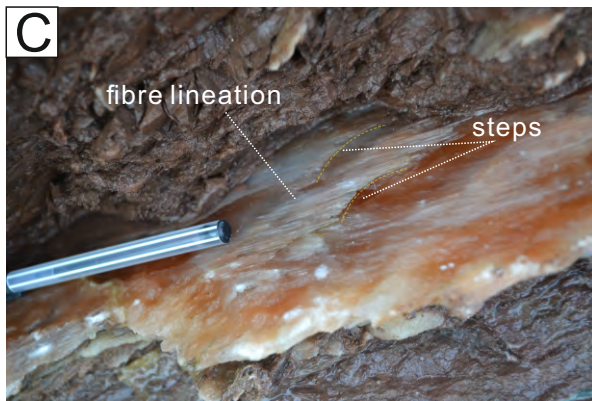
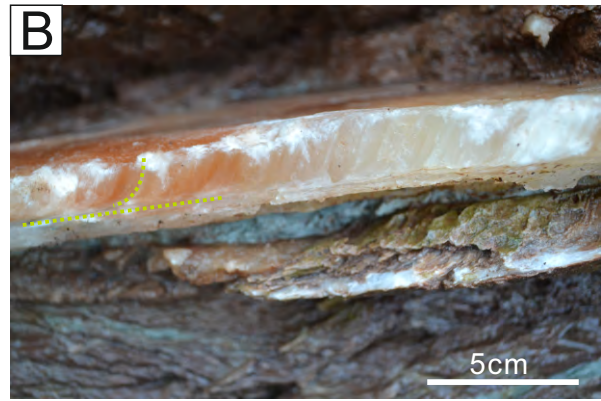
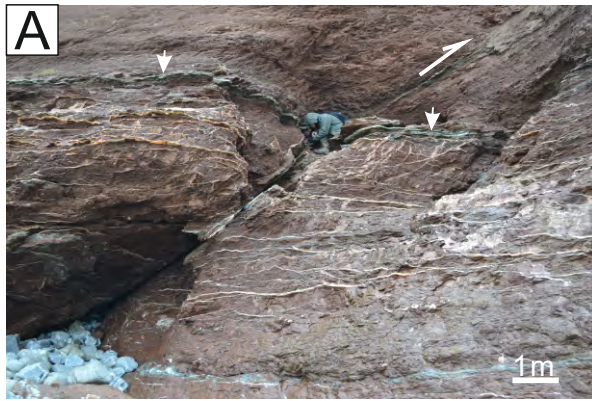


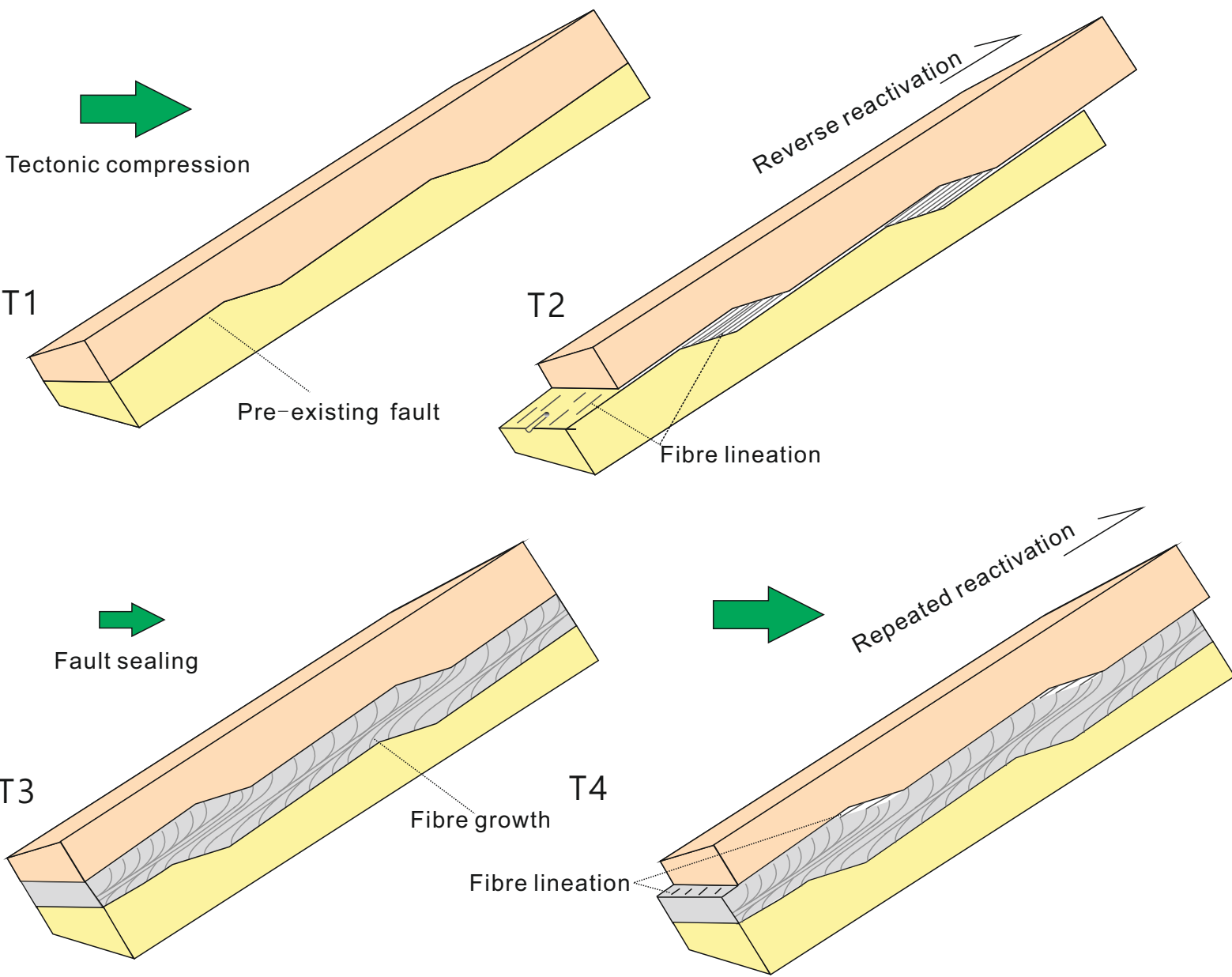


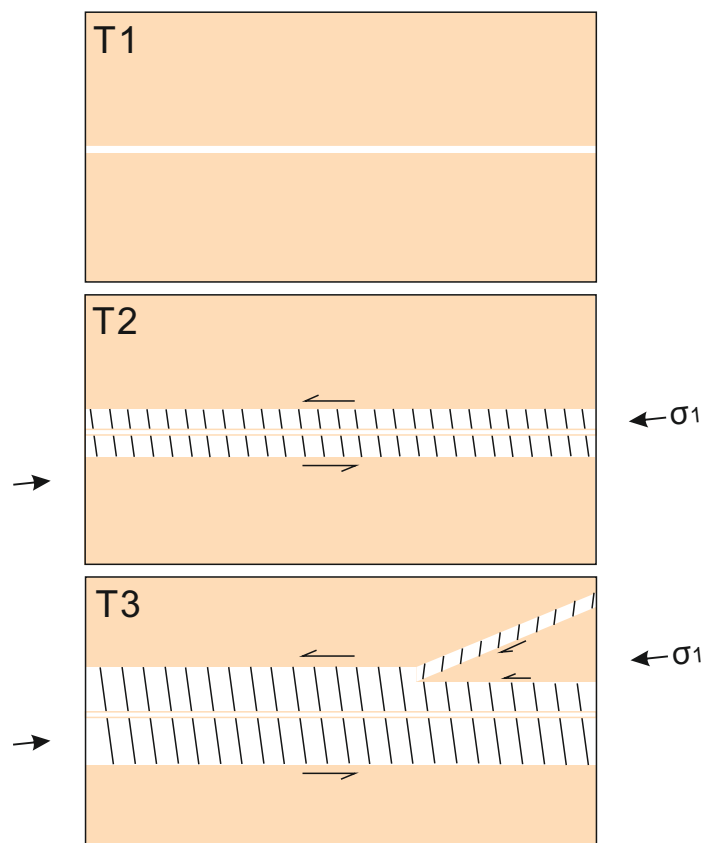












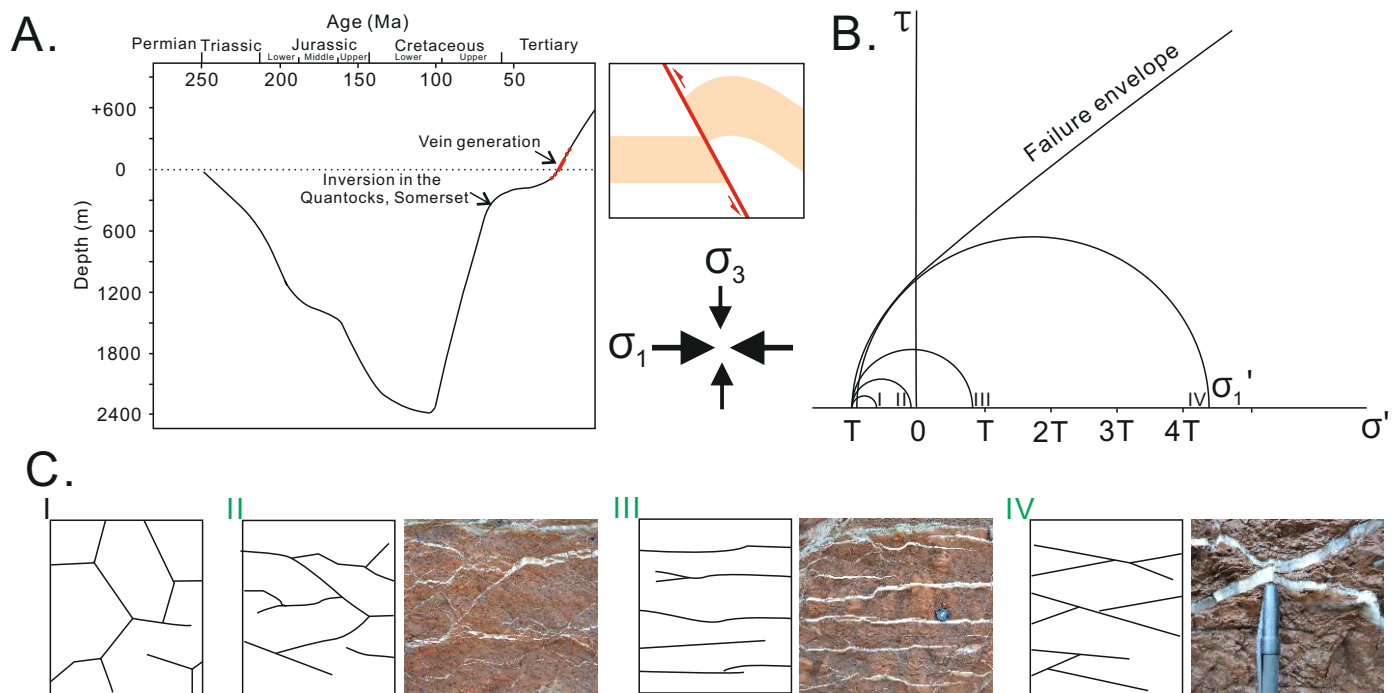


Table 1. Data for sandstone dykes of the Mercia Mudstone in study area. HGV, horizontal gypsum veins. IGV, inclined gypsum veins.

No.	Dip direction (°)	Dip angle (°)	Trace length (m)	Aperture (cm)	UTM Coordinates			Notes
					Northing	Easting	Zone	
SD1	52	74	2.9	8.2	5670202	476345	30U	see Fig. 3B
SD2	71	84	6.1	7.8	5670188	476263	30U	see Fig. 3A
SD3	52	75	2.8	6.6	5670184	476251	30U	curved shape, cross-cut by HGV
SD4	61	70	0.6	8.2	5670184	476251	30U	curved shape, cross-cut by HGV
SD5	99	41	0.8	1.2	5670176	476233	30U	cross-cut by HGV
SD6	232	74	0.7	1.6	5670169	476202	30U	cross-cut by nodule-rooted HGV
SD7	78	37	6.4	14.6	5670139	476061	30U	cross-cut by HGV and IGV
SD8	122	50	2.8	16.8	5670119	476019	30U	see Fig. 3C
SD9	56	59	4.0	22.5	5670114	476010	30U	cross-cut by HGV and IGV
SD10	71	56	0.3	2.2	5670113	476007	30U	cross-cut by HGV
SD11	68	64	0.6	2.0	5670113	476007	30U	cross-cut by HGV
SD12	70	60	0.4	0.8	5670113	476007	30U	cross-cut by HGV